

The Effects and Implications of Oxidation on Nuclear Grade Graphite

A Thesis

Presented in Partial Fulfillment of the Requirements for the

Degree of Master of Science

with a

Major in Mechanical Engineering

in the

College of Graduate Studies

University of Idaho

by

Austin C. Matthews

Major Professor: Richard Christensen, Ph.D.

Committee Members: Will Windes, Ph.D.; Michael McKellar, Ph.D.

Department Administrator: Gabriel Potirniche, Ph.D.

December 2020

**Authorization to Submit Thesis**

This thesis of Austin Matthews, submitted for the degree of Master of Science with a Major in Mechanical Engineering and titled "The Effects and Implications of Oxidation on Nuclear Grade Graphite," has been reviewed in final form. Permission, as indicated by the signatures and dates below, is now granted to submit final copies to the College of Graduate Studies for approval.

Major Professor: \_\_\_\_\_ Date: \_\_\_\_\_

Richard Christensen, Ph.D.

Committee Members: \_\_\_\_\_ Date: \_\_\_\_\_

Will Windes, Ph.D.

\_\_\_\_\_ Date: \_\_\_\_\_

Michael McKellar, Ph.D.

Department

Administrator: \_\_\_\_\_ Date: \_\_\_\_\_

Gabriel Potirniche, Ph.D.

## Abstract

Graphite is an important and often life-limiting component for reactors using graphite components. It is used as a structural and moderating material in both research and commercial high-temperature gas cooled reactor designs. Prior to use in a reactor, the physical, mechanical, and thermal properties of the selected graphite grade must be assessed to evaluate the in-service performance over the life of the component. While graphite is inherently stable in the inert environment of a helium-cooled reactor during normal operations (anticipated 400–1000°C core temperature), graphite is susceptible to rapid oxidation when exposed to oxidizing conditions at these operating temperatures. The concern with oxidation is its impact on the physical, mechanical, and thermal properties of graphite. Changes to the structural integrity of the core components is the most critical safety issue for reactors, meaning any changes in mechanical strength of the graphite components can affect the core safety analysis and must be determined for a variety of oxidizing conditions. Also critical is the impact of oxidation on physical and thermal properties, a decrease in the density of graphite due to oxidation for example will decrease neutron moderation and affect the neutronic efficiency of the core physics. Additionally, the rate of heat removal from fuel can be significantly impacted as the thermal diffusivity decreases with oxidation.

The strength behavior of fine- and medium-grain nuclear graphite grades are examined following exposure to varying oxidizing conditions within the kinetic regime as defined by the ASTM oxidation test standard 7542. This study addresses the critical issue of remaining oxidized material properties of graphite core components after oxidized mass losses up to and beyond the current limits recommended within the ASME Boiler and Pressure Vessel (BPV) code (implied maximum mass loss = 10%) over a range of oxidation temperatures from 550°C to 750°C. Preliminary results generally demonstrate that low-temperature oxidation can result in 30% greater strength reductions than is seen during oxidation at higher temperatures with similar mass-loss levels. These results have implications in the way the ASME BPV code is currently interpreted, as there is no provision for the oxidizing conditions which were found to have a significant effect on the strength of graphite after oxidation.

Property changes of fine- and medium-grain nuclear graphite grades are examined after subsection to uniform oxidation conditions within the kinetic regime as defined by the ASTM oxidation test standard 7542. This study addresses the underlying physical property changes of nuclear-graphite components for oxidized mass losses beyond the current limits recommended for

graphite components in the ASME code. Property measurements include density, elastic modulus, shear modulus, coefficient of thermal expansion, electrical resistivity, and thermal diffusivity. Preliminary results demonstrate a decrease in elastic modulus and thermal diffusivity, and an increase in electrical resistivity and coefficient of thermal expansion with increasing oxidation mass loss. The decrease in coefficient of thermal expansion contradicts previous work due to differing oxidation regimes and highlights a need for clarity in the ASME Boiler and Pressure Vessel code on the way oxidation occurs.

### **Acknowledgements**

I would like to thank Will Windes and Dave Swank for their seemingly endless guidance and support through the process. I would also like to thank David Cottle for all his help with property measurements, even when they were not so straightforward.

Funding for this work was provided by the Department of Energy's Advanced Reactor Development (ARD) program under the DOE Idaho Operations Office, Contract DE-AC07-05ID14517 with Battelle Energy Alliance, LL

**Dedication**

I would like to thank my mom, who believes I can do anything even when I don't.

## Table of Contents

|  |          |
|--|----------|
| Authorization to Submit Thesis.....  | ii       |
| Abstract.....  | iii      |
| Acknowledgements.....  | v        |
| Dedication.....  | vi       |
| Table of Contents.....   | vii      |
| List of Figures.....   | x        |
| List of Tables.....  | xii      |
| <b>CHAPTER 1. BACKGROUND AND MOTIVATION.....</b>   | <b>1</b> |
| 1.1. Graphite use in the Nuclear Industry.....   | 1        |
| 1.2. ASME BPV Code Requirements and Concerns.....  | 2        |
| 1.2.1. Oxidized Strength.....  | 2        |
| 1.2.2. Oxidized Material Properties.....   | 3        |
| 1.3. Graphite Oxidation Regimes.....   | 4        |
| 1.4. References.....   | 6        |
| <b>CHAPTER 2. THE DEGRADATION OF STRENGTH UNDER VARYING OXIDIZING CONDITIONS FOR<br/>NUCLEAR GRAPHITE.....</b> | <b>8</b> |
| 2.1. Introduction.....   | 8        |
| 2.2. Experimental.....   | 9        |
| 2.2.1. Specimen Information.....   | 9        |
| 2.2.2. Specimen Preparation.....   | 10       |
| 2.2.3. Oxidation.....  | 10       |
| 2.2.4. Mechanical Testing.....   | 12       |
| 2.2.5. Optical Analysis.....   | 13       |

|   |  |    |
|---|--|----|
| 2.3.  | Results .....                                    | 15 |
| 2.3.1.  | Mechanical Testing .....                         | 15 |
| 2.3.2.  | Image Analysis.....                              | 16 |
| 2.4.  | Discussion.....                                  | 19 |
| 2.4.1.  | Trends in Strength vs Oxidation Data .....       | 19 |
| 2.4.2.  | Application of Results.....                      | 20 |
| 2.5.  | Conclusions .....                                | 21 |
| 2.6.  | References.....                                  | 22 |
| CHAPTER 3. THERMAL AND PHYSICAL PROPERTY CHANGES UNDER UNIFORM OXIDATION IN<br>NUCLEAR GRAPHITE ..... |  | 25 |
| 3.1.  | Introduction .....                               | 25 |
| 3.2.  | Experimental .....                               | 25 |
| 3.2.1.  | Specimen Information.....                        | 25 |
| 3.2.2.  | Specimen Preparation.....                        | 26 |
| 3.2.3.  | Oxidation.....                                   | 26 |
| 3.2.4.  | Property Testing.....                            | 27 |
| 3.2.4.1.  | Density.....                                     | 28 |
| 3.2.4.2.  | Elastic Modulus from Sonic Velocity .....        | 28 |
| 3.2.4.3.  | Elastic Modulus from Fundamental Frequency ..... | 30 |
| 3.2.4.4.  | Coefficient of Thermal Expansion .....           | 32 |
| 3.2.4.5.  | Electrical Resistivity.....                      | 33 |
| 3.2.4.6.  | Thermal Diffusivity .....                        | 35 |
| 3.3.  | Results .....                                    | 37 |
| 3.3.1.  | Elastic Modulus from Sonic Velocity .....        | 37 |
| 3.3.2.  | Elastic Modulus from Fundamental Frequency ..... | 38 |
| 3.3.3.  | Coefficient of Thermal Expansion .....           | 39 |

|            |  |    |
|------------|--|----|
| 3.3.4.     | Electrical Resistivity .....           | 39 |
| 3.3.5.     | Thermal Diffusivity .....              | 40 |
| 3.4.       | Discussion.....                        | 41 |
| 3.4.1.     | Elastic Modulus .....                  | 41 |
| 3.4.2.     | Coefficient of Thermal Expansion ..... | 41 |
| 3.4.3.     | Electrical Resistivity.....            | 42 |
| 3.4.4.     | Thermal Diffusivity .....              | 42 |
| 3.5.       | Conclusions .....                      | 43 |
| 3.6.       | References.....                        | 44 |
| CHAPTER 4. | CONCLUSIONS .....                      | 46 |
| 4.1.       | Strength After Oxidation .....         | 46 |
| 4.2.       | Properties After Oxidation .....       | 46 |
| 4.3.       | ASME BPV Code Concerns.....            | 47 |

## List of Figures

|  |    |
|--|----|
| Figure 1.1: ASME Normalized Strength vs Weight Loss (reproduced from American Society of Mechanical Engineers, BPVC 2019).....                                   | 3  |
| Figure 1.2: Previous work showing no change in CTE with oxidation (Hacker et al. 2000) .....   | 4  |
| Figure 1.3: Walker diagram showing graphite oxidation regimes (Windes et al. 2014).....  | 5  |
| Figure 2.4: Apparatus for oxidizing graphite samples.....  | 12 |
| Figure 5.2: Failures typical of untrimmed (left) and trimmed (right) samples. ....   | 13 |
| Figure 2.6: Optical analysis procedure.....  | 14 |
| Figure 2.7: Trimming evaluations for Grade IG-110 (top) and NBG-18 (bottom) at 650°C. Blue lines indicate approximate trimming location of 3mm from the end..... | 15 |
| Figure 2.8: Normalized failure stress vs. mass loss. ....  | 16 |
| Figure 2.9: Radial porosity profiles for IG-110 (left) and NBG-18 (right) at various temperatures. ...   | 18 |
| Figure 3.10: Apparatus for oxidizing graphite samples.....   | 27 |
| Figure 3.11: Sonic velocity measurement station.....   | 29 |
| Figure 3.12: Fundamental frequency measurement station. ....   | 31 |
| Figure 3.13: Commercial push rod Dilatometer for CTE measurement. ....   | 33 |
| Figure 3.14: Electrical resistivity measurement station.....   | 34 |
| Figure 3.15: LFA measurement station for determination of thermal diffusivity. ....  | 36 |
| Figure 3.16: Shear modulus from sonic velocity.....  | 37 |
| Figure 3.17: Young’s modulus from sonic velocity.....  | 38 |
| Figure 3.18: Young’s modulus from fundamental frequency .....  | 38 |
| Figure 3.19: Coefficient of thermal expansion.....   | 39 |
| Figure 3.20: Electrical resistivity .....  | 40 |
| Figure 3.21: Thermal diffusivity through LFA.....  | 40 |

Figure 3.22: Average CTE from 20-600° C as a function of weight loss for 2 different graphites

(Hacker et al. 2000) ..... 42

**List of Tables**

|  |    |
|--|----|
| Table 2.1: Properties of Examined Graphites. ....  | 9  |
| Table 2.2: Specimen oxidation plan. Numbers represent samples tested for IG-110 and NBG-18 grades..... | 10 |
| Table 3.3: Properties of Examined Graphites .....  | 25 |

## CHAPTER 1. BACKGROUND AND MOTIVATION

### 1.1. Graphite use in the Nuclear Industry

Traditionally, the United States nuclear industry has used light water reactors (LWR) for their power generation needs. However, with the existing aging nuclear infrastructure and limits of traditional LWRs, the Department of Energy (DOE) has invested in research and development for next generation nuclear reactor technology. The DOE's Generation IV Nuclear Energy Systems Program initially decided to pursue five different reactor concepts to determine which was the most appropriate to meet the future power concerns of the United States. Due to its high technology maturity they decided to pursue the Very High Temperature Reactor (VHTR) concept as a means of producing safe and reliable energy. (Corwin et al., 2008) The VHTR concept has many advantages over traditional LWR designs. One of the biggest advantages of the newer helium cooled designs is that the technology is inherently safe. LWR designs are limited in output temperature to around 300°C while VHTR technology can provide process heat with coolant outlet temperatures in excess of 1000°C. This process heat can be used for applications such as coal gasification, hydrogen production, and water desalination, along with providing higher efficiency to the attached power cycle. (Corwin et al., 2008; Piore and Duffey, 2019) However, to achieve these higher outlet temperatures and higher efficiencies, a robust structural material is required.

In most reactors, neutrons need to be reduced in energy before they can continue the chain of fission. This is achieved by causing atomic collisions and interactions between the neutrons and a material known as a moderator. A moderator is typically a light element, such as water or carbon. As graphite is composed of carbon it can be used as an effective moderator. Graphite is a desirable material for reactor core components as it is readily available, relatively inexpensive, easy to machine, and sufficiently strong to be used in structural applications. (Burchell et al., 1991) Modern nuclear graphites are also of high purity with low elemental contamination. This ensures little interference with the neutronics of a reactor and allows for easier disposal of graphite components at end of life as it largely does not activate under irradiation. Additionally, graphite is very thermally stable (stable > 2500°C) and has been found to increase its strength with increasing temperature well beyond the peak temperatures of a core in accident conditions. (Zhou et al., 2017) A combination of these properties mean graphite is an ideal material choice for reactor components. The drawback of using graphite is how little is known about its material properties, especially after

degradation occurs through irradiation and oxidation. Much of the prior work examining the strength of graphite after oxidation follows no accepted standards or does not investigate the effects of varying oxidation conditions. (Collins et al., 1965; Eto and Growcock, 1983; Price and Beavan, 1981 ) There is little previous work on the thermal and physical properties of graphite after oxidation and much of the work that has been done doesn't take into account how varying oxidizing conditions effect such properties. (Hacker et al. 2000) This work focuses on how the mechanical, physical, and thermal properties of certain nuclear grade graphites change after oxidation, and how the oxidizing conditions can affect those changes.

## **1.2. ASME BPV Code Requirements and Concerns**

One of the primary goals of this work is to inform the American Society of Mechanical Engineers (ASME) Boiler & Pressure Vessel (BPV) code of potential issues with the interpretation and implementation of the code for addressing oxidation degradation of graphite components. The BPV code will be used heavily in the development of new reactor technology and it must be specific enough to capture the required material properties and how they will change without being so constricting that the research required before attempting to build a new reactor becomes prohibitively exhaustive.

### **1.2.1. Oxidized Strength**

According to the ASME BPV code, "the region where strength decreases to less than 50% shall not be credited in the stress evaluation." The code then provides a figure, reproduced in Figure 1, which shows that the strength of oxidized graphite decreases to ~50% of its original value at 10% weight loss. (American Society of Mechanical Engineers, 2019) This means any graphite oxidized to 10% weight loss is assumed to have zero strength in the stress evaluation. While this guidance is a conservative approach to determine the effects of oxidation it is not supported by direct experimental data and requires further research. This research will demonstrate that while sometimes this is a reasonable conservative approximation, other times oxidized graphite retains a very high portion of its strength at 10% weight loss depending on graphite grade and oxidation condition.

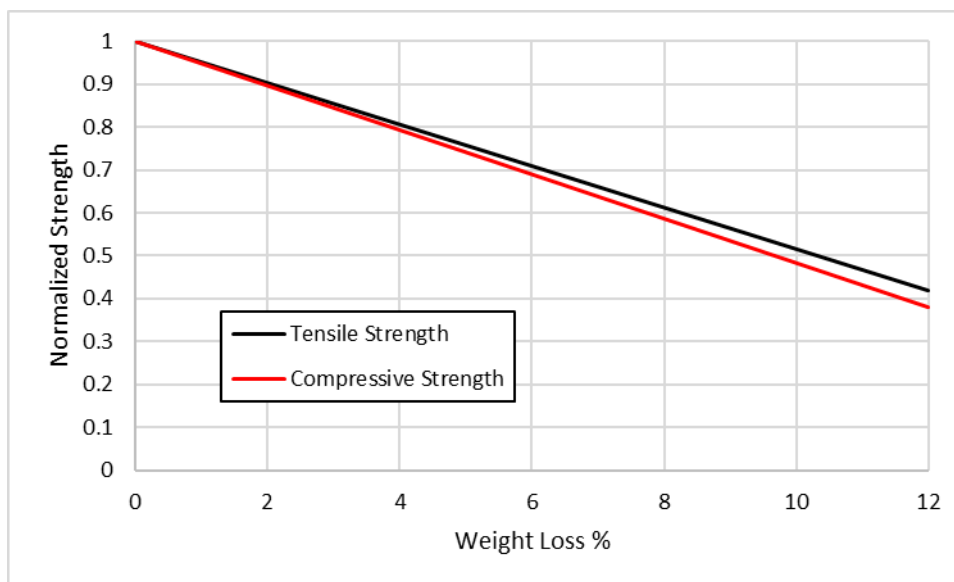


Figure 1.1: ASME Normalized Strength vs Weight Loss (reproduced from American Society of Mechanical Engineers, BPVC 2019)

Additionally, the code does not specifically define how oxidation weight loss should be used to determine component degradation. For example, 10% weight loss for an outer reflector block component away from the core center region may be completely irrelevant to the function of the reactor whereas 10% weight loss for a component providing access to a control rod may lead to component failure and prevent insertion of a control rod during an off-normal event. It is also possible to look at all the graphite in discrete volumes, when a certain volume reaches 10% weight loss, it is no longer assumed to have any strength. But that also has issues with sizing of the discrete volumes and more importantly, how oxidation weight loss is measured on many discrete volumes inside of an operating reactor.

### 1.2.2. Oxidized Material Properties

ASME only currently requires the elastic modulus and thermal conductivity as a function of temperature up to 10% weight loss. This work will show that while these properties are important, there are additional properties that change with oxidation under certain conditions which need to be accounted for when designing graphite components. While the primary issues in the ASME code for residual strength after oxidation are not present for other material properties after oxidation, there are issues with the data that have been previously collected for these properties. Very little data have been collected on the properties of graphite after oxidation and the studies that have been performed have found no change in the coefficient of thermal expansion of graphite with

increasing oxidation, shown in Figure 1.2. (Hacker et al. 2000) The research conducted by Hacker et al. was by no means incorrect, however the way graphite is oxidized affects the properties of the graphite after oxidation. This work will illustrate why oxidation material properties changes may not always be representative of how graphite will oxidize in a reactor and may not be applicable to the requirements specified in the ASME code.

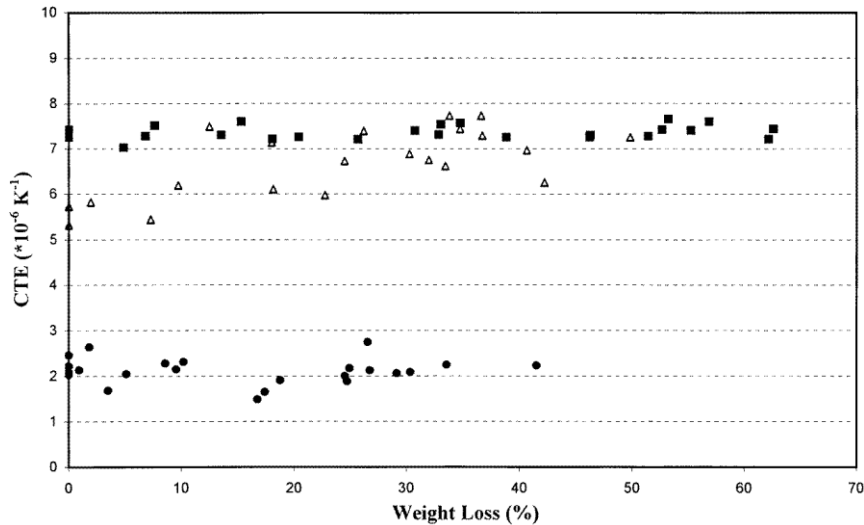


Figure 1.2: Previous work showing no change in CTE with oxidation (Hacker et al. 2000)

### 1.3. Graphite Oxidation Regimes

One of the main challenges with conducting research on graphite oxidation is the variability of the effect of oxidation depending on the oxidation conditions including oxidant, temperature, and specimen size and geometry. This section will describe how graphite oxidizes in air at different temperatures using the Walker diagram shown in Figure 1.3.

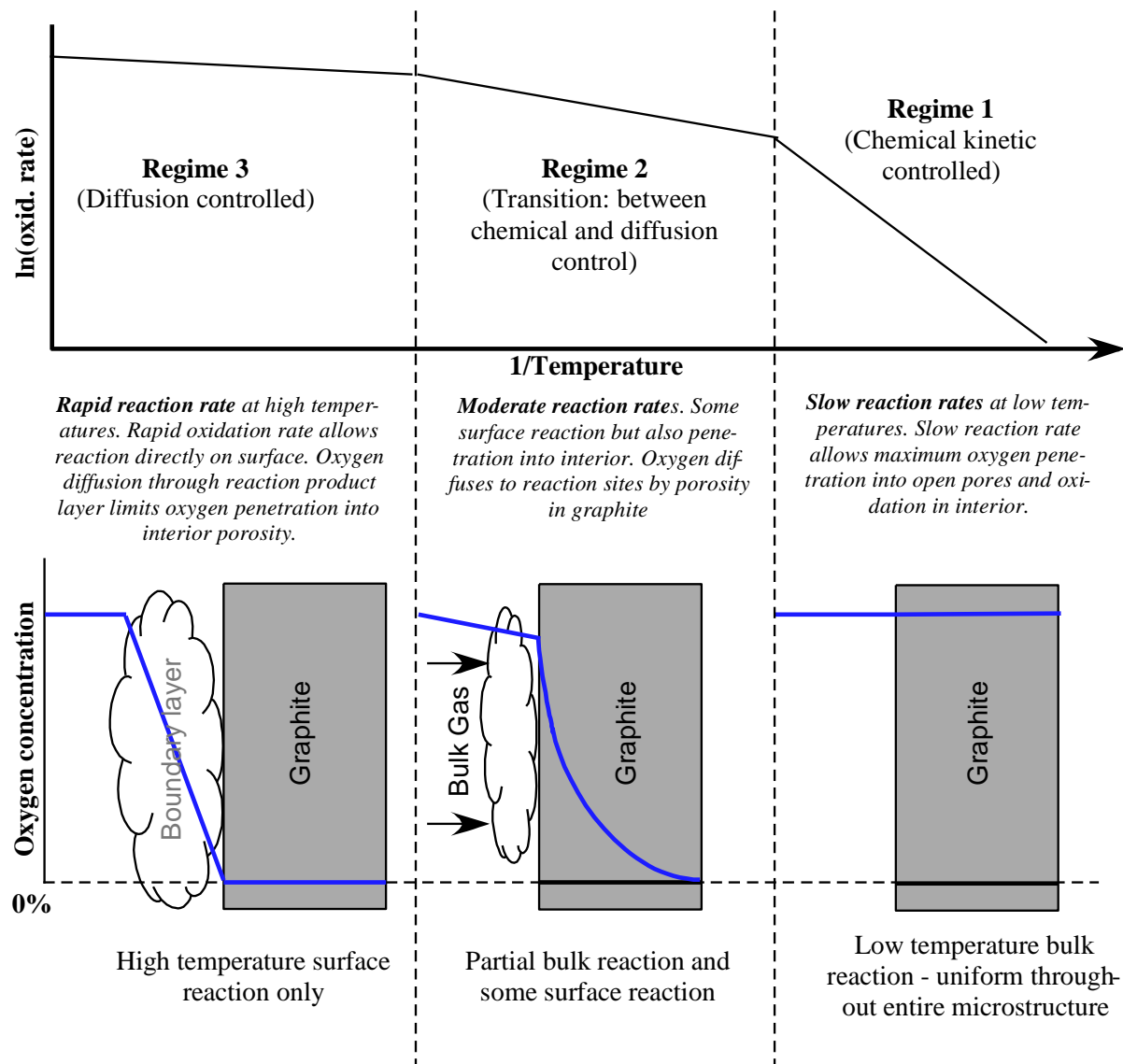


Figure 1.3: Walker diagram showing graphite oxidation regimes (Windes et al. 2014)

At lower temperatures, below  $650^{\circ}\text{C}$ , behavior in regime 1 in Figure 1.3 is observed. The reaction rate between the oxygen and the carbon in the graphite is slow enough that the oxygen can diffuse into the structure of the graphite uniformly before reacting. This results in a uniform oxygen concentration throughout the graphite and in turn, uniform oxidation. This is referred to as the kinetically controlled regime as it is limited by reaction kinetics. (Windes et al. 2014)

As the temperature increases to a range from  $650^{\circ}\text{C}$  to  $750^{\circ}\text{C}$ , the reaction rate between the carbon and the oxygen increases until the oxygen can no longer uniformly diffuse through the graphite before reacting. This results in a gradient of oxygen concentration and in turn, a gradient of oxidation in the graphite. This is represented by regime 2 in Figure 1.3. In this transition regime,

the oxidation rate begins to be governed by the rate of oxygen diffusion into the graphite rather than the rate of the reaction between carbon and oxygen. (Windes et al. 2014)

At higher temperatures, above 750°C, regime 3 from Figure 1.3 is observed. At these temperatures, the chemical reaction between carbon and oxygen occurs much more rapidly than the diffusion of oxygen through the graphite, resulting in the majority of oxidation occurring on the outer surface of the graphite. This is referred to as the diffusion-controlled regime, as the oxidation reaction occurs as quickly as oxygen can reach active sites on the surface of the graphite. (Windes et al. 2014)

In chapter 2 oxidation was conducted targeting each of these 3 regimes to examine the differences between them. In chapter 3 oxidation was conducted with the intent of remaining in the purely kinetically controlled regime to ensure uniform oxidation that would yield valid property measurements of the bulk material.

#### **1.4. References**

American Society of Mechanical Engineers, 2017 ASME Boiler & Pressure Vessel Code: An International Code, Section III: Rules for Construction of Nuclear Facility Components, Division 5: High Temperature Reactors, New York, NY: ASME, 2017.

Breeze, P., "Nuclear Power," Power Generation Technologies (Third Edition), 2019.

Burchell, T.D., Fuller, E. L., Romanoski, G.R., and Strizak, J.P., "Graphite for the Nuclear Industry," 1991.

Collins, A.C., Masterson, H.G., and Jennings, P.P., "The effect of oxidation on the compressive strength of graphite," Journal of Nuclear Materials, vol. 15, no. 2, pp. 135-136, 1965.

Corwin, W.R., Burchell, T.D., Katoh, Y., McGreevy, T.E., Nanstad, R.K., Ren, W., Snead, L.L., and Wilson, D.F., "Generation IV Reactors Integrated Materials Technology Program Plan: Focus on Very High Temperature Reactor Materials," Oak Ridge National Laboratory, 2008.

Eto, M. and Growcock, F.B., "Effect of oxidizing environment on the strength of H451, PGX and IG-11 graphites," Carbon, vol. 21, no. 2, pp. 135-147, 1983.

Hacker, P.J., Neighbour, G.B., and McEnaney, B, "The coefficient of thermal expansion of nuclear graphite with increasing thermal oxidation," J. Phys. D: Appl. Phys. 33, pp.991-998, 2000.

Pioro, I., Duffey, R., "Current and future nuclear power reactors and plants," Managing Global Warming, 2019.

Price, R.J. and Beavan, L.A., "Strength of Nonuniformly Oxidized PGX Graphite," General Atomic Co., San Diego, 1981.

Windes, W., Strydom, G., Smith, R., and Kane, J., "Role of Nuclear Grade Graphite in Controlling Oxidation in Modular HTGRs," Idaho National Laboratory, 2014.

Zhou, X., Tang, Y., Lu, Z., Zhang, J., and Liu, B., "Nuclear graphite for high temperature gas-cooled reactors," *New Carbon Materials*, vol. 32, no. 3, pp. 193-204, 2017.

## CHAPTER 2. THE DEGRADATION OF STRENGTH UNDER VARYING OXIDIZING CONDITIONS FOR NUCLEAR GRAPHITE

### 2.1. Introduction

The U.S. Advanced Reactor Technologies Graphite Research and Development Program is conducting extensive graphite-oxidation experiments, both chronic and acute, to provide oxidation behavior data to assist in the prediction of graphite-component performance after oxidation with a specific emphasis on data accounting for the impact of oxidation rate and oxidation behavior to assist in determining the changes to the structural integrity of graphite core components. Because graphite-component strength is a critical parameter necessary to determine core structural integrity, determining the actual residual strength after oxidation is essential for determining component oxidation limits within the American Society of Mechanical Engineers (ASME) design code. This study specifically addresses acute oxidation in the presence of molecular oxygen and its impact on the degradation behavior of nuclear graphite. The following work is directly applicable to ASME code specifications for future HTR license applications which will require similar information.

The ASME Boiler Pressure Vessel Code, specifying requirements for use of graphite components in nuclear applications, requires a potential reactor vendor to perform oxidation testing on each specific graphite grade to be used in the reactor core. (American Society of Mechanical Engineers, 2019). ASME code states that the region where strength decreases to less than 50% shall not be credited in the stress evaluation and provides figure HHA-3141-1 which illustrates normalized strength as a function of graphite weight loss. According to this guidance, any component over ~10% mass loss is assumed to have zero strength in the stress evaluation. While clear in intent, there are multiple somewhat subtle but unresolved issues with this assumption. A few examples include: (1) How should mass loss be calculated? Should mass loss be calculated as a function of the entire core or for individual components?; (2) Do all oxidizing conditions have the same impact on strength?; (3) Can actual strength loss be used rather than a conservative assumption of zero strength after 10% mass loss? This study is intended to provide direct measurement and provide some guidance for addressing the above unresolved issues. In turn this will allow the community to address these ASME code questions and to begin providing specific guidance to the HTR licensing and design community.

The initial motivation for this work is based on the premise that strength degradation in graphite with oxidation will depend upon the oxidizing environment. Unique microstructural

features within each graphite grade influence the macroscopic (or bulk) oxidation-reaction rate. Simply put, the rate is dependent upon relative concentration of active sites (Chi et al., 2008; Contescu et al., 2012; Kane et al., 2017; Kyotani et al., 1993; Laine et al., 1963; Lizzo et al. 1990) within the graphite and transport efficiency, which is strongly influence by pore morphology and size. Both are unique to each graphite grade and dependent on source feedstock materials and processing. (American Society for Testing and Materials, 2008; Kelly, 1981; Nightingale, 1962, Choi et al., 2011; El-Genk and Tournier, 2012, 2011; Kane et al., 2018). The dominance of one factor over the other can have a significant impact on where oxidation occurs. At one extreme, oxidation could be uniform (low reactivity and high mass transport efficiency), and the total measured mass loss would be identical to the local mass loss throughout the oxidized material. At the other extreme, oxidation will occur primarily on the surface of the component with the total mass loss reaching 10% but the interior would remain nearly identical to the unoxidized graphite.

## 2.2. Experimental

Cylindrical specimens with dimensions appropriate for compression testing were machined from fine-grain and medium-grain size graphite grades. Oxidized specimens were tested within the kinetic controlled oxidation temperature range (550°C – 750°C) over a total mass loss range of 0% to ~10% using established standardized test methods. After oxidation, compressive mechanical strength at each mass loss were measured for all specimens. The residual compressive strength after oxidation, at different temperatures, for medium and fine-grained grades were compared to ascertain the effects of oxidation.

### 2.2.1. Specimen Information

Two nuclear graphite grades were tested. Grade IG-110 is a super-fine-grain graphite, fabricated from petroleum coke using an iso-molding fabrication process. NBG-18 was originally designed and fabricated by SGL Carbon for the South African Pebble Bed Modular Reactor and is a medium grain graphite. It is fabricated from pitch (coal-tar) coke using a vibrational molding process. These grades and select nominal properties are listed in Table 2.1.

Table 2.1: Properties of Examined Graphites.

| Grade  | Vendor     | Grain Designation | Grain Size         | Coke Type | Fabrication Method | Density <sup>c</sup> (g/cm <sup>3</sup> )<br>$\mu \pm \sigma$ |
|--------|------------|-------------------|--------------------|-----------|--------------------|---|
| IG-110 | Toyo Tanso | Super-fine        | 20 $\mu\text{m}^b$ | Petroleum | Iso-molded         | 1.774 $\pm$ 0.002   |

|   |     |        |                     |       |              |              |
|---|-----|--------|---------------------|-------|--------------|--------------|
| NBG-18  | SGL | Medium | 1.6 mm <sup>a</sup> | Pitch | Vibra-molded | 1.852 ±0.004 |
| a. Manufacturer's nominal maximum grain size.<br>b. Manufacturer's nominal average grain size.<br>c. Density values listed are specific to samples examined in this work. |     |        |                     |       |              |              |

Due to the grain sizes used for each respective grade IG-110 has a very fine pore structure while NBG-18 has a much larger pore microstructure. Both grades represent distinctly different fabrication processes, raw materials, and microstructures. They also represent relative extremes in oxidation rates among common nuclear graphites and provide a good comparison of oxidation behavior.

### 2.2.2. Specimen Preparation

A total of 36 cylindrical samples were prepared from each grade, with dimensions of 25.4 mm (1 in) diameter by 50.8 mm (2 in) height. Thirty-one samples of each grade were then oxidized according to Table 2, while five specimens from each grade were left unoxidized. After oxidation, specimens were mechanically tested in compression with the five unoxidized specimens for each grade providing the as-received (as-fabricated) mechanical-strength values.

Table 2.2: Specimen oxidation plan. Numbers represent samples tested for IG-110 and NBG-18 grades.

| Oxidation Temperature (°C) | Nominal Mass Loss |    |     |
|----------------------------|-------------------|----|-----|
|                            | 0%                | 5% | 10% |
| 550                        | 5                 | 5  | 5   |
| 650                        |                   | 5  | 6*  |
| 750                        |                   | 5  | 5   |

\* One specimen selected for optical image analysis

### 2.2.3. Oxidation

An American Society of Testing and Materials (ASTM) standardized test (ASTM D7542) is available for oxidation rate testing over the temperature range of 500–750°C. Testing under the conditions specified by this standard is intended to ensure a controlled oxidation and repeatable oxidation environment. Controlled oxidation is achieved by providing an abundant and uniform oxidation environment within the controlled temperature regime (i.e., 500–750°C). While the

oxidation conditions used for this study follow the intent of the ASTM D7542 standard, the tests were modified to accommodate multiple specimens oxidizing under the same conditions rather than only one test specimen being oxidized at a time.

Graphite oxidation was performed using a custom apparatus built at Idaho National Laboratory, Figure 2.4. The apparatus was designed to create a uniform and abundant air flow over multiple specimens in compliance with the intent of ASTM D7542. (American Society for Testing and Materials, 2015a) Dry air flowed through a porous, sintered quartz frit to provide a uniform plug airflow gas environment over all samples. A quartz “grill” minimized surface contact between the frit and the test samples while minimizing airflow disturbance. All oxidation was carried out in model BF51894C-1 Linberg/Blue M Moldatherm box furnaces with an air flow rate of 10 standard liters per minute using an Alicat model MC-10SLPM-DI5M mass-flow controller. The incoming air was pre-heated by passing it through a coil of tubing inside the furnace prior to entering the oxidation apparatus. Temperatures were measured using a Type K thermocouple held adjacent to the graphite samples. Measured specimen temperatures for the nominal 550, 650, and 750°C oxidation conditions were 546, 659, and 759°C, respectively. The estimated interfacial gas velocity at 10 standard liters per minute was 67 mm/second.

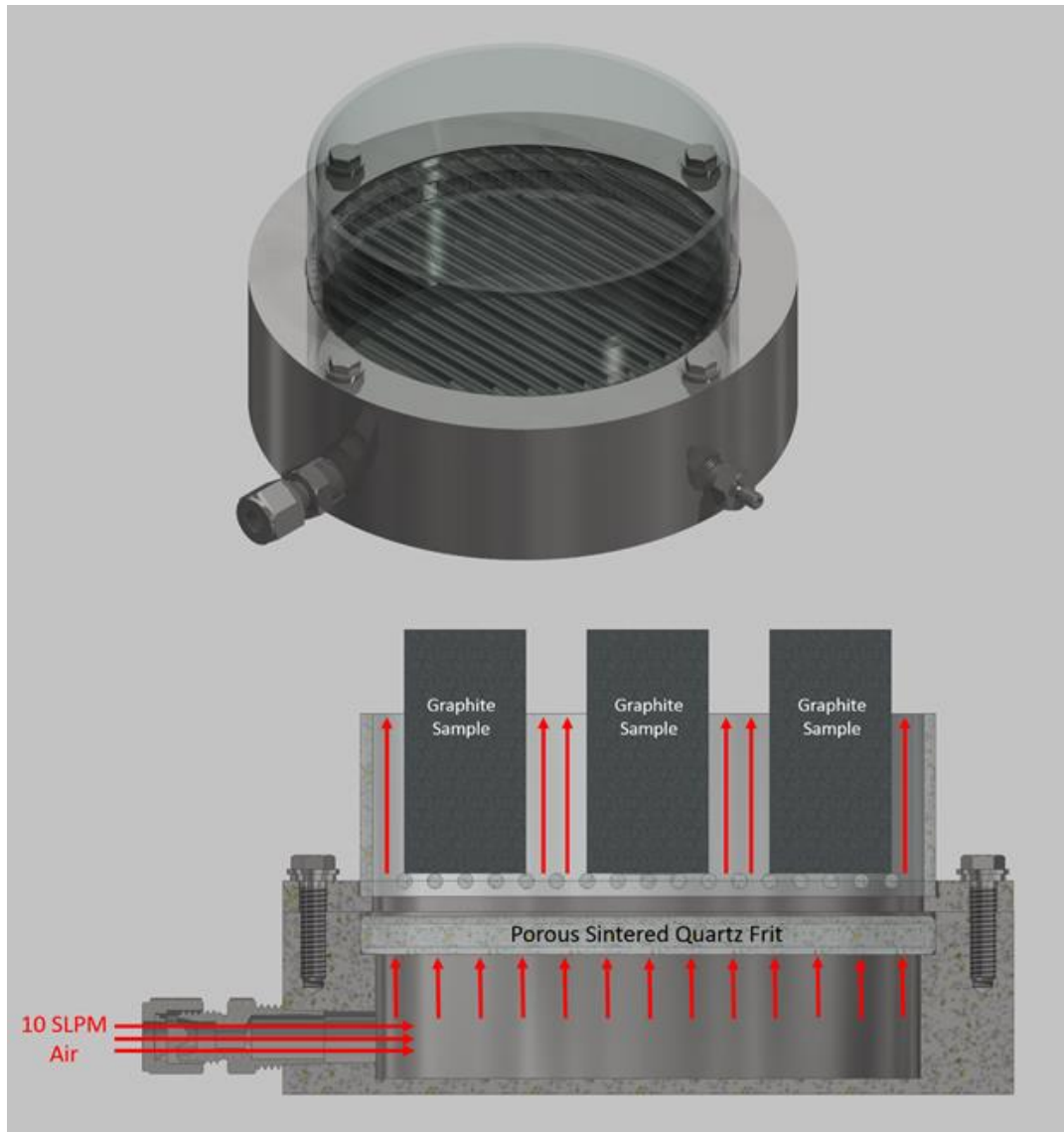


Figure 2.4: Apparatus for oxidizing graphite samples.

#### 2.2.4. Mechanical Testing

After oxidation, compressive mechanical strength was measured for all specimens. All mechanical testing was performed at room temperature on an Instron model 5582 electromechanical load frame using an Instron 63209 100 kN static load cell. All tests were performed using Instron Bluehill 3 software with a crosshead speed of 1 mm/min.

Currently, no approved ASTM test standard for mechanical testing of oxidized graphite exists. Testing was conducted using the approved ASTM test standard C695 with the following exceptions (American Society for Testing and Materials, 2015b):

- C695 requires a height-to-diameter ratio between 1.9 and 2.1. Samples had a height-to-diameter ratio between 1.75 and 1.8 after they were trimmed (discussed below).
- C695 requires all surfaces to have a surface finish visually comparable to 0.8  $\mu\text{m}$  root mean square or better. Samples met this requirement on the ends of the cylinders after they were trimmed. Faces of the cylinders were left as oxidized and did not meet this requirement.

Initial mechanical testing showed failures atypical of as-fabricated graphite material (Figure 5). These failures along the edges of the cylindrical specimens indicated that the material was failing within the loaded volume directly adjacent to the ends of the specimens, rather than transferring the entire applied stress evenly throughout the specimens as required in ASTM C695. Two factors were assumed to contribute to these problems. First, the oxidation profile at the specimen ends will not be uniform due to accelerated oxidation within the corners as a result from higher rate of oxygen transfer from the external surfaces on the ends and the radial side simultaneously. Second, oxidation resulted in uneven surfaces where the loading platens contact the samples, resulting in uneven loading. To mitigate these issues, a 3 mm-wide section was trimmed from both ends of all samples to remove the layer of highest mass loss and to generate a flat surface. This trimming procedure ensured the applied stress was distributed uniformly throughout the specimen interior, rather than propagating cracks within the local volume adjacent the cylinder edges. A similar technique has been utilized previously with good results. (Zhou et al., 2017)



Figure 5.2: Failures typical of untrimmed (left) and trimmed (right) samples.

### 2.2.5. Optical Analysis

One sample of each grade from the 650°C and 10% mass-loss testing condition was sectioned to perform optical image analysis on the interior microstructure of the specimens. Only the 650°C case was examined because the lower temperature was assumed to approach uniform oxidation, while the higher temperature oxidation will have a smaller penetration depth. Optical analysis was

undertaken to determine the approximate oxidation penetration depth to help interpret mechanical strength behavior and to verify that the trimming technique removed the region of highest damage from the ends of the samples.

The sample was sectioned and polished prior to microscopy. The procedure for polishing is described subsequently with ultra-sonic cleaning in water taking place between each step:

- Polishing down to 600 grit on SiC paper
- Polishing with 9  $\mu\text{m}$  polycrystalline diamond on a nylon polishing cloth
- Polishing with 3  $\mu\text{m}$  polycrystalline diamond on a nylon polishing cloth
- Polishing with 0.05  $\mu\text{m}$  alumina on a neoprene polishing cloth.

Composite bright field images were captured with a Keyence VHX-6000 digital microscope. The image was converted to greyscale then to binary (black and white) using a filter that changes all pixels above a certain greyscale value to white and all pixels below this value to black. The columns of the binary image were then averaged to give a fraction of the image that was white (indicating a pore) and plotted to show a general trend of porosity as seen in Figure 2.6: Optical analysis procedure. This method is dependent on image quality and is not intended to be a comprehensive evaluation of the complete porosity; however, it is a good representation of the porosity gradient for images collected at identical conditions.

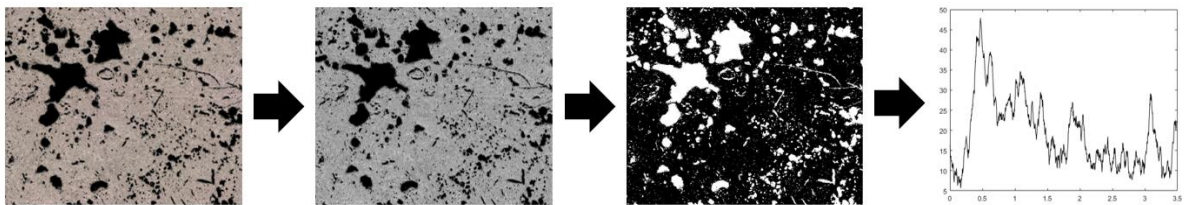


Figure 2.6: Optical analysis procedure.

Results from the optical analysis demonstrate the maximum oxidation occurred within 3mm of the edges for these 650°C samples, Figure 2.7. These results were used to confirm the depth necessary for trimming the ends of the samples to eliminate the majority of the oxidation degraded volume.

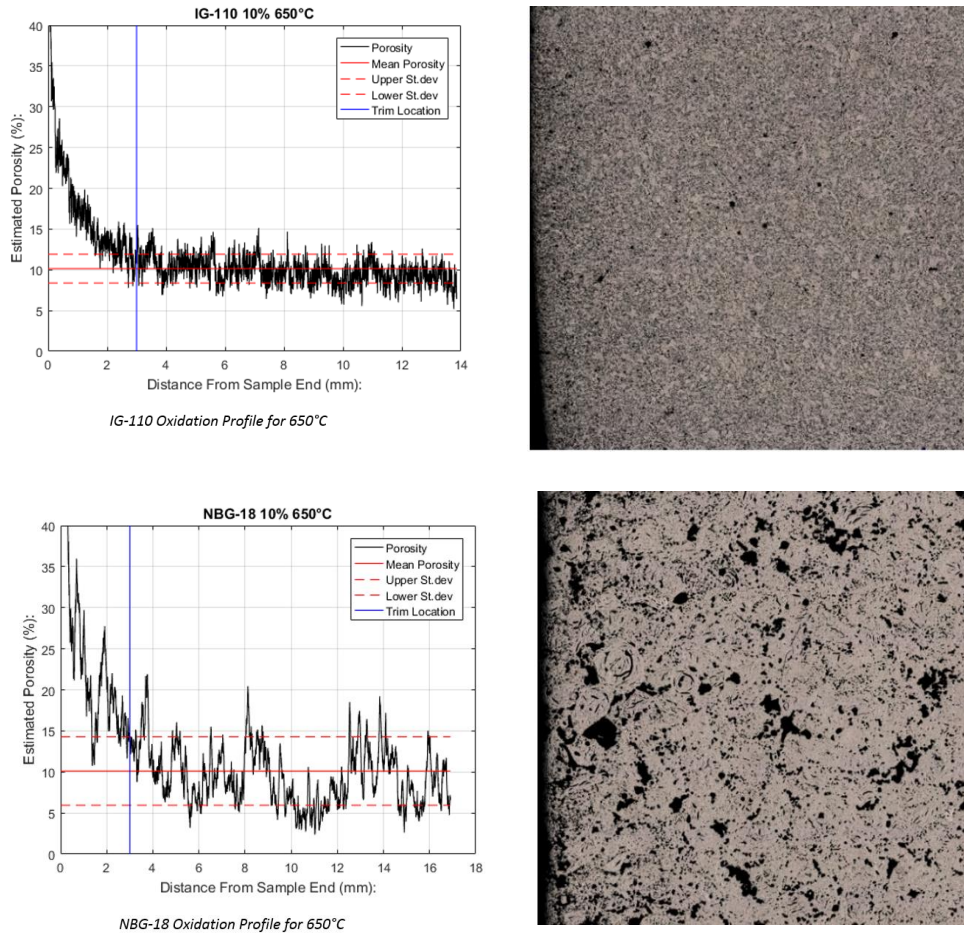


Figure 2.7: Trimming evaluations for Grade IG-110 (top) and NBG-18 (bottom) at 650°C. Blue lines indicate approximate trimming location of 3mm from the end.

### 2.3. Results

Mechanical-failure stresses were recorded for all oxidation mass-loss levels for IG-110 and NBG-18 to ascertain the effects of oxidation on the residual strength on these fine- and medium-grained graphite grades. Oxidation profiles from optical imaging, as well as mechanical test results for all samples were analyzed.

#### 2.3.1. Mechanical Testing

Oxidized failure stress as a fraction of unoxidized failure stress ( $\sigma_{ox}/\sigma_{unox}$ ) is plotted against oxidized mass-loss percentage for all graphite specimens (Figure 2.8). Colors correspond to oxidation temperatures (Red = 750°C, Green = 650°C, and Blue = 550°C). Hollow markers indicate IG-110 and solid markers indicate NBG-18. The arrows were included to highlight the trends between the higher temperature (red) and the lower temperature samples (blue, green). The

failure stress for both grades is shown to decrease with increasing oxidation. However, the failure stress appears to be dependent on oxidation temperature with the general trend showing higher failure stress for high temperatures and lower failure stress for low temperatures.

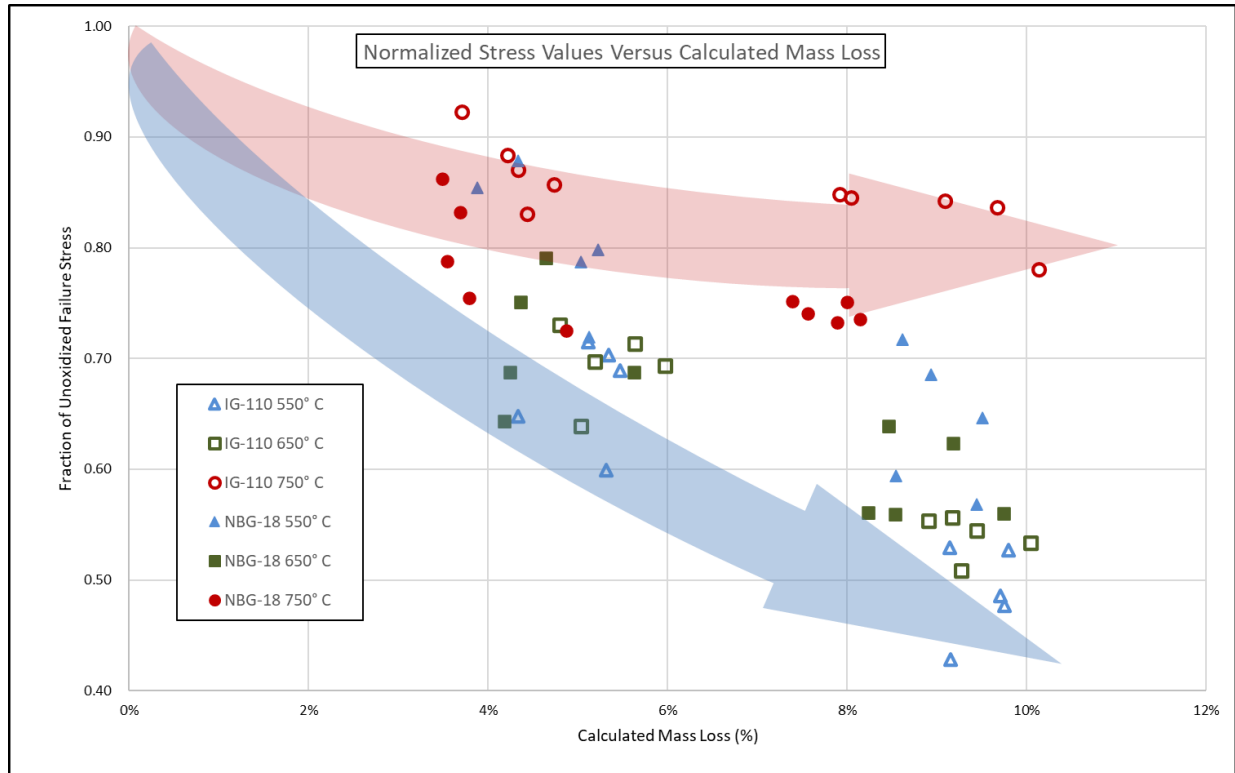


Figure 2.8: Normalized failure stress vs. mass loss.

### 2.3.2. Image Analysis

The radial porosity profiles generated after oxidation for both grades at each oxidation temperature are shown in Figure 2.9. The lower-temperature oxidation demonstrates uniform, kinetically controlled oxidation providing a lower reaction rate and, thus, a high penetration depth into the graphite microstructure. Higher-temperature diffusion-controlled oxidation provides a high reaction rate where the outer layers of graphite are oxidized rapidly, with only limited penetration into the microstructure. The 650°C middle temperature demonstrates an intermediate behavior, having a gradual porosity profile, but also a significant damaged layer near the exterior surface of the samples.

The lower temperature 550°C oxidation shows no real visible line of penetration depth, verifying uniform oxidation throughout the entire graphite microstructure. Conversely, the 750°C oxidation exhibits a rapid change in total porosity from the exterior surface to a small distance into

the bulk volume (a very small penetration-depth profile) with minimal oxidation occurring in the center of the samples, verifying the rapid diffusion-controlled oxidation behavior. The image analysis results align closely with expectations and allow for better interpretation of the mechanical testing results.

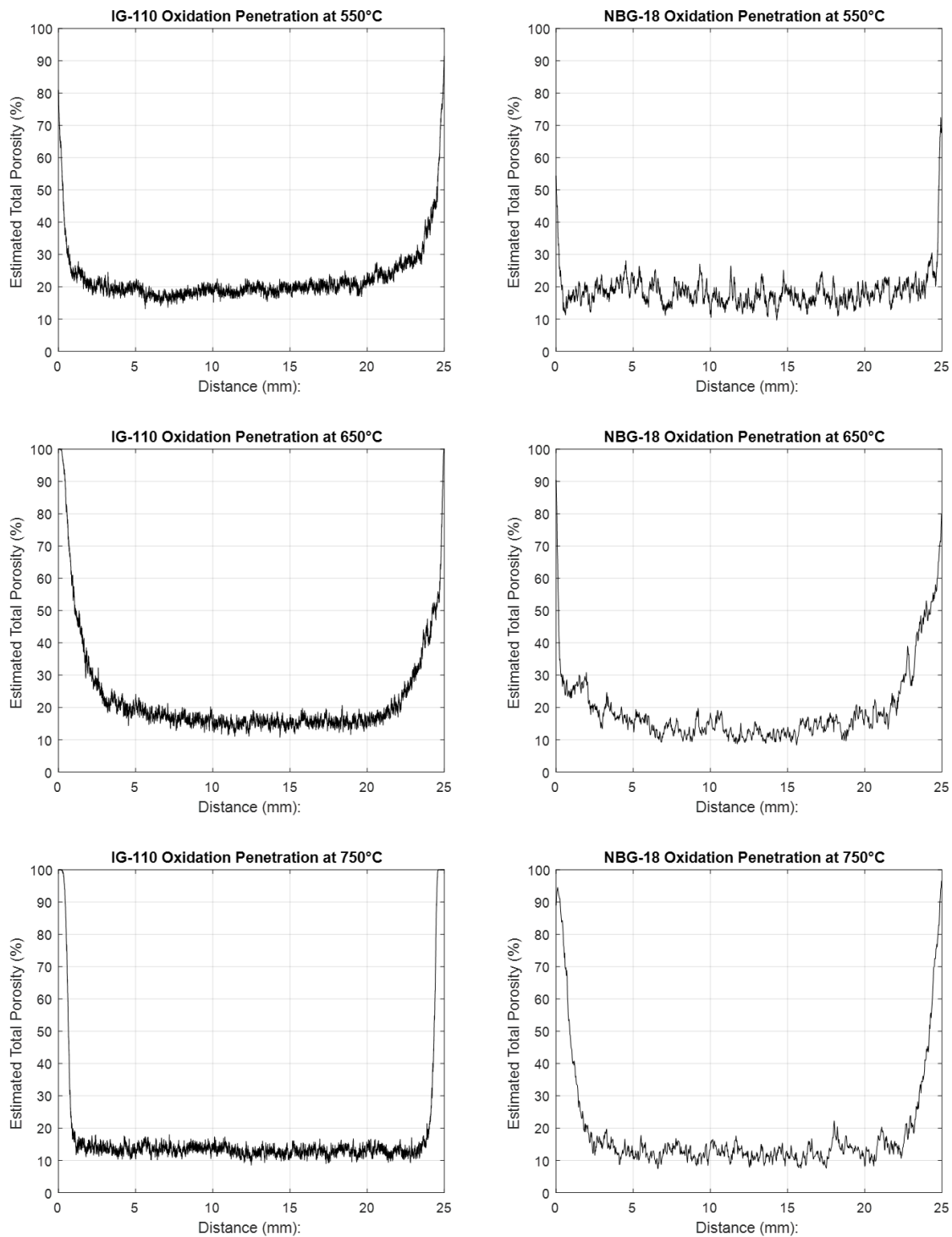


Figure 2.9: Radial porosity profiles for IG-110 (left) and NBG-18 (right) at various temperatures.

## 2.4. Discussion

The graphite oxidation and post-oxidation mechanical data are herein discussed. These results are compared to the observations from optical image analysis for all oxidation temperatures tested.

### 2.4.1. Trends in Strength vs Oxidation Data

As expected, mechanical strength decreased with increased oxidation of graphite specimens at all temperatures. However, many previous studies have largely ignored or found no effect of oxidation temperature on graphite strength (Collins et al., 1965; Eto and Growcock, 1983; Peng, 1979, 1977; Price and Beavan, 1981), leaving a need for understanding the effect of oxidation temperature on failure stress. As seen in Figure 2.8, several interesting mechanical behaviors are noted; the 750°C conditions have the highest retained failure stress over all mass loss values for both fine-grain and medium-grain size grades. The decrease in failure stress from 5% to 10% mass loss at a given temperature is very similar between grades at the high and low temperatures.

- High temperature oxidation (750°C) yields highest failure stress values.
- Low temperature oxidation (550°C) yields lower failure stress values.
- Oxidation at 650°C is within the transition-temperature regime (between mostly diffusion-controlled and kinetic-controlled oxidation). Because oxidation behavior is microstructure dependent, the oxidation behavior for each grade at these intermediate temperatures can vary. It is difficult to determine definite trends between grades at this temperature.
- At 5% mass loss the oxidation profile is not fully developed and is at different stages of development between the two grades, resulting in a discontinuity in the trends between the 5% and 10% results. Future work will focus on extending to higher mass loss values to verify these observed trends.
- Trimming of the sample ends is necessary to perform an accurate mechanical strength test as optical analysis observed the development of surface irregularities which may lead to regions of high stress. (Kane et al., 2017; Xiaowei et al., 2004, Zhou et al., 2017)

It is seen both in the strength values in Figure 2.8 and oxidation profile plots in Figure 2.9, that oxidation porosity occurs much differently between the two grades. This is most easily observed under the 650°C conditions. The difference in tested oxidized strength values can be attributed to

the difference in oxygen penetration depth within the microstructure. Many factors affect oxygen penetration including sample size, sample geometry, and of course the unique microstructure for each grade. (Kane et al., 2017)

The microstructural difference between grades is the largest factor affecting their oxidation behavior. From previous oxidation studies, IG-110 has demonstrated a much higher effective diffusion coefficient than NBG-18, (Kane et al., 2018) which implies oxygen can more easily penetrate the graphite. NBG-18 has a higher overall density, larger grain size, and a lower open-pore density than IG-110, which may significantly affect the differences between oxidation-penetration depths at a given temperature. (Chi and Kim, 2008) Together, these microstructural differences can be attributed to the difference in oxidation profile and the resultant difference in failure-load decrease between the two grades.

#### **2.4.2. Application of Results**

While the results from this work are geometry dependent and not directly scalable to larger components, they nevertheless contain vital information for reactor designers. This study clearly demonstrates the residual strength of graphite after oxidation does not depend solely on mass loss, but also on oxidation temperature and oxidant availability. Figure 2.8 illustrates that at 10% mass loss, a graphite grade can lose 15–50% (or more) of its as-fabricated strength, depending on the temperature to which it is exposed during oxidation.

Current ASME code assumes zero strength at ~10% mass loss when performing probability of failure analysis, regardless of oxidation temperature. (American Society of Mechanical Engineers, 2017) These results indicate that oxidation effects must be carefully considered by graphite core designers and should be addressed within the ASME code-development activities. This conclusion is especially valid with respect to the large components expected to be used within a new HTR core design. The ASME code must address the penetration depth and variable strength issues that have been raised within this study. This study also illustrates that further work is necessary in determining *where* the oxidation occurs within an HTR core and what the effects will be for larger graphite components. However, no guidance on how the mass loss should be achieved is provided. Because this work shows that the oxidation temperature is critical to determining residual strength within oxidized components, consideration as to where the oxidation degradation might occur within the graphite core must be addressed. For example, if oxidation only occurs within the hottest region of the core, and the oxidation is assumed to be diffusion-controlled, then the

structural integrity of the core components should be calculated differently from components suffering oxidation degradation at lower temperatures outside of this central hot core zone.

## 2.5. Conclusions

Several interesting results have been observed with this study, both in oxidation behavior and the effects on mechanical strength. Differences are attributed to oxidation temperature, graphite microstructures, and pore microstructures. The major conclusions are summarized as:

The mechanical strength decreased with oxidation of the graphite specimens at all temperatures.

Strength changes tended to vary due to oxidation temperature. The general trends noted for oxidation temperature dependency are:

- a. Specimens oxidized at the highest temperature (750°C) which is the most aggressive oxidation condition, yield higher failure-stress values than specimens oxidized to similar mass loss levels at lower temperatures.
- b. Specimens oxidized at the lowest temperature (550°C) demonstrated lower strength values than specimens oxidized to similar mass-loss levels at the highest temperatures.
- c. Specimens oxidized at 650°C showed a mixed behavior, with the medium-grained grade (NBG-18) showing lower failure-stress values than their counterpart 550°C specimens, and the fine-grained grade (IG-110) demonstrating higher strength values than did the 550°C specimens.

Oxidation and strength changes behave differently between the two grades. As discussed in the 650°C oxidation conditions, this is attributed to the difference in oxygen-penetration depth within the unique graphite microstructure.

Optical-image results inform and confirm the influence that unique graphite microstructure has on the effects of oxidation.

- a. 550°C oxidation demonstrates uniform porosity.
- b. 750°C oxidation demonstrates “shrinking core” oxidation.
- c. The 650°C middle temperature demonstrates an intermediate behavior, having a gradual porosity profile but also a significantly damaged layer near the surface of the specimens.

Current ASME code assumes zero calculated strength at ~10% mass loss regardless of oxidation temperature which may be overly conservative.

## 2.6. References

American Society for Testing and Materials, "ASTM C695-15 Standard Test Method for Compressive Strength of Carbon and Graphite," 2015b.

American Society for Testing and Materials, "ASTM D7219, Standard Specification for Isotropic and Near-isotropic Nuclear Graphites," 2008.

American Society for Testing and Materials, "ASTM D7542, Standard Test Method for Air Oxidation of Carbon and Graphite in the Kinetic Regime," 2015a.

American Society of Mechanical Engineers, 2017 ASME Boiler & Pressure Vessel Code: An International Code, Section III: Rules for Construction of Nuclear Facility Components, Division 5: High Temperature Reactors, New York, NY: ASME, 2017.

Burchell, T. and Bratton, R., "NGNP Graphite Testing and Qualification Specimen Selection Strategy," Idaho National Laboratory, 2005.

Burchell, T., Bratton, R., and Windes, W., "NGNP Graphite Selection and Acquisition Strategy," Oak Ridge National Laboratory, 2007.

Chi, S. and Kim, G., "Comparison of the oxidation rate and degree of graphitization of selected IG and NBG nuclear graphite grades," *Journal of Nuclear Materials* Volume 381, pp. 9-14, 2008.

Choi, E.Y., San Choi, W., Lee, Y.B., and Noh, Y.Y., "Production of graphene by exfoliation of graphite in a volatile organic solvent," *Nanotechnology*, vol. 22, no. 36, 2011.

Collins, A.C., Masterson, H.G., and Jennings, P.P., "The effect of oxidation on the compressive strength of graphite," *Journal of Nuclear Materials*, vol. 15, no. 2, pp. 135-136, 1965.

Contescu, C., Guldán, T., Wang, P., and Burchell, T., "Effect of microstructure on air oxidation resistance of nuclear graphite," *Carbon*, vol. 50, pp. 3354-3366, 2012.

Contescu, C.I., Azad, S., Miller, D., Lance, M.J., Baker, F.S., and Burchell, T.D., "Practical aspects for characterizing air oxidation of graphite," *Journal of nuclear materials*, vol. 381, no. 1-2, pp. 15-24, 2008.

El-Genk, M.S. and Tournier, J.P., "Development and validation of a model for the chemical kinetics of graphite oxidation," *Journal of Nuclear Materials*, vol. 411, no. 1-3, pp. 193-207, 2011.

El-Genk, M.S. and Tournier, J.P., "Validation of gasification model for NBG-18 nuclear graphite," *Nuclear Engineering and Design*, vol. 250, pp. 142-155, 2012.

Eto, M. and Growcock, F.B., "Effect of oxidizing environment on the strength of H451, PGX and IG-11 graphites," *Carbon*, vol. 21, no. 2, pp. 135-147, 1983.

Geschwindt, J., Lommers, L., Southworth, F., and Shahrokhi, F., "Performance and optimization of an HTR cogeneration system," *Nuclear Engineering and Design*, vol. 251, 2012.

Harvego, E.A., Reza, S.M.M., Richards, M., and Shenoy, A., "An evaluation of reactor cooling and coupled hydrogen production processes using the modular helium reactor," *Nuclear Engineering and Design*, vol. 236, pp. 1481-1489, 2006.

Idaho National Laboratory, "PLN-2497, Graphite Technology Development Plan", 2010.

Kane, J.J., Contescu, C.I., Smith, R.E., Strydom, G., and Windes, W.E., "Understanding the reaction of nuclear graphite with molecular oxygen: kinetics, transport, and structural evolution," *J. Nucl. Mater* 493, pp. 343-367, 2017.

Kane, J.J., Matthews, A.C., Orme, C.J., Contescu, C.I., Swank, W.D., and Windes, W.E., "Effective gaseous diffusion coefficients of select ultra-fine, super-fine and medium grain nuclear graphite," *Carbon Volume 136*, pp. 369-379, 2018.

Kelly, B.T., "Physics of Graphite," Applied Sciences Publishers LTD, London, 1981.

Kyotani, T., Leon Y Leon, C.A., and Radovic, L.R., "Simulation of carbon gasification kinetics using an edge recession model," *AIChE journal*, vol. 39, no. 7, pp. 1178-1185, 1993.

Laine, N.R., Vastola, F.J., and Walker Jr., P.L., "The importance of active surface area in the carbon-oxygen reaction1, 2," *The Journal of physical chemistry*, vol. 67, no. 10, pp. 2030-2034, 1963.

Lizzio, A., Jiang, H., and Radovic, L.R., "On the kinetics of carbon (char) gasification: reconciling models with experiments," *Carbon*, vol. 28, no. 1, pp. 7-19, 1990.

Nightingale, R.E., *Nuclear Graphite*, Academic Press, ISBN: 978-1-4832-2854-9, 1962.

Patterson, M.W., "Cogeneration of electricity and liquid fuels using a high temperature gas-cooled reactor as the heat source," *Nuclear Engineering and Design*, vol. 329, pp. 204-212, 2018.

Peng, T., "Effects of Oxidation on the Mechanical Properties of Carbon/Graphite," in *Carbon*, Irvine, CA, 1977.

Peng, T., "Oxidation effects on the tensile strength of ATJS graphite and vitreous carbon," *Carbon*, vol. 17, no. 2, pp. 157-174, 1979.

Price, R.J. and Beavan, L.A., "Strength of Nonuniformly Oxidized PGX Graphite," General Atomic Co., San Diego, 1981.

Walker Jr., P.L., Rusinko Jr., F., and Austin, L.G., "Gas Reactions of Carbon," *Advances in Catalysis*, vol. 11, pp. 133-221, 1959.

Wichner, R.P., Burchell, T.D., and Contescu, C.I., "Penetration depth and transient oxidation of graphite by oxygen and water vapor," *Journal of Nuclear Materials*, vol. 393, no. 3, pp. 518-521, 2009.

Xiaowei, U., Jean-Charles, R., and Suyuan, Y., "Effect of temperature on graphite oxidation behavior," *Nuclear Engineering and Design*, vol. 227, no. 3, pp. 273-280, 2004.

Zhou, X., Contescu, C.I., Zhao, X., et al., "Oxidation Behavior of Matrix Graphite and Its Effect on Compressive Strength," *Science and Technology of Nuclear Installations*, 2017.

## CHAPTER 3. THERMAL AND PHYSICAL PROPERTY CHANGES UNDER UNIFORM OXIDATION IN NUCLEAR GRAPHITE

### 3.1. Introduction

The U.S. Advanced Reactor Technologies Graphite Research and Development Program is conducting extensive graphite-oxidation experiments, both chronic and acute, to provide oxidation-behavior data to assist in the prediction of graphite-component performance after oxidation with a specific emphasis on data accounting for the impact of oxidation rate and oxidation behavior to assist in determining the changes to the structural integrity of graphite core components. This study specifically addresses chronic oxidation in the presence of molecular oxygen and its impact on the degradation of material properties of nuclear graphite. The following work is directly applicable to ASME code specifications for future HTR license applications which will require similar information.

### 3.2. Experimental

Graphite samples were oxidized at a low oxidation temperature to specific mass loss intervals. Material property tests were performed on a set of unoxidized samples and then repeated for the oxidized samples for each mass loss interval. Graphite oxidation was designed to ensure a large penetration depth within the samples and completely uniform oxidation profile throughout the graphite microstructure. Therefore, all samples were oxidized within the kinetic-controlled regime at low temperatures and an oxygen-rich atmosphere

#### 3.2.1. Specimen Information

Two nuclear-graphite grades currently under consideration by commercial HTR vendors were tested. Grade IG-110 is a super-fine-grain grade, fabricated from petroleum coke using an iso-molding fabrication process. NBG-18 is a medium grain grade, fabricated from pitch (coal) coke using a vibrational molding process. These grades and select nominal properties are listed in Table 2.1.

Table 3.3: Properties of Examined Graphites

| Grade  | Vendor     | Grain Designation | Grain Size                  | Coke Type | Fabrication Method | Density <sup>c</sup> (g/cm <sup>3</sup> )<br>$\mu \pm \sigma$ |
|--------|------------|-------------------|-----------------------------|-----------|--------------------|---|
| IG-110 | Toyo Tanso | Super-fine        | 20 $\mu\text{m}^{\text{b}}$ | Petroleum | Iso-molded         | 1.79  |
| NBG-18 | SGL        | Medium            | 1.6 mm <sup>a</sup>         | Pitch     | Vibra-molded       | 1.86  |

- a. Manufacturer's nominal maximum grain size.
- b. Manufacturer's nominal average grain size.
- c. Density values listed are specific to samples examined in this work.

Due to the grain sizes used for each respective grade, IG-110 has a very fine pore structure, while NBG-18 has a much larger pore microstructure. Both grades represent distinctly different fabrication processes, raw materials, and microstructures that provide a good comparison of oxidation behavior between the available nuclear-graphite grades.

### **3.2.2. Specimen Preparation**

A total of 6 samples were prepared from each grade in 2 different specimen geometries. 3 samples were made at 12.7 mm (0.5 in) diameter by 25.4 mm (1 in) height and 3 samples at 12.7 mm (0.5 in) diameter by 6.35 mm (0.25 in) height. The shorter samples were required for thermal diffusivity measurements and the longer samples were used in all other material property testing. All samples were oxidized to 5% mass loss increments and property tests were conducted at each increment.

### **3.2.3. Oxidation**

Specimen oxidation was performed using a custom apparatus built at Idaho National Laboratory (INL), Figure 2.4. The apparatus was designed to create a uniform flow of air over multiple specimens in compliance with ASTM D7542. (American Society for Testing and Materials, 2015) Dry air flows through a porous, sintered quartz frit to provide a uniform plug airflow gas environment over all samples. A quartz grill minimizes surface contact between the frit and the test samples with minimal airflow disturbance. All oxidation was carried out in model BF51894C-1 Linberg/Blue M Moldatherm box furnaces with an air flow rate of 10 standard liters per minute using an Alicat model MC-10SLPM-DI5M mass-flow controller. The incoming air was heated by flowing through a coil of tubing inside the furnace prior to entering the oxidation apparatus. Temperature was measured using a Type K thermocouple held adjacent to the graphite samples. Oxidation occurred at 485° C and is expected to be uniform oxidation in the kinetic regime.

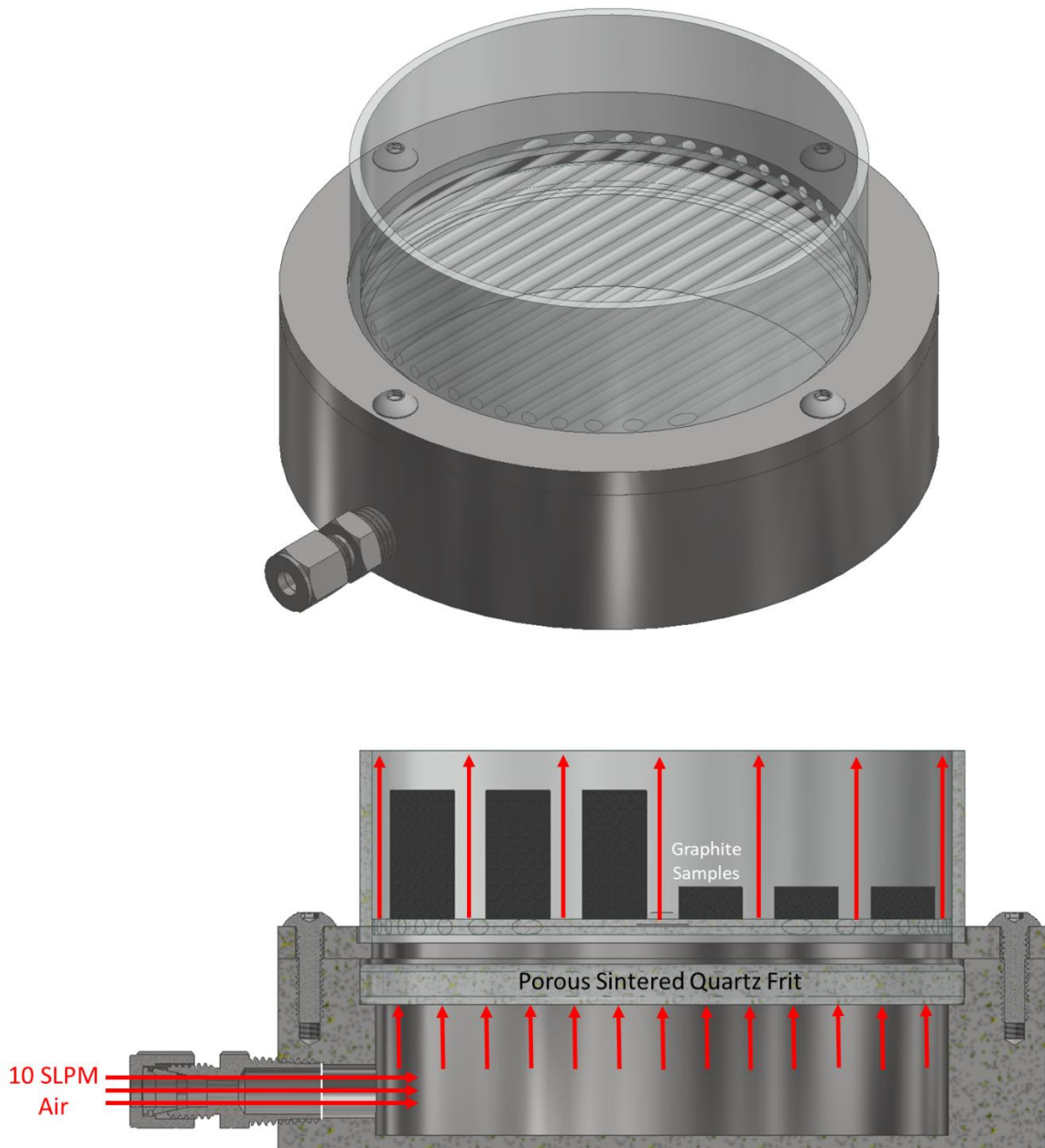


Figure 3.10: Apparatus for oxidizing graphite samples.

#### 3.2.4. Property Testing

Precision and bias have been conducted for all ASTM standards and is discussed within each test standard. The precision and error levels for using these standards for the sample geometries

used in this study are bound within the considerable variability of the graphite material. (Swank et al. 2012)

#### **3.2.4.1. Density**

Dimensional and mass measurements are performed to ASTM Standard C559-90, which describes in detail the procedure for performing dimensional measurements and calculating bulk density. All dimensional measurements of the specimen radius and length were performed with calibrated micrometers and calipers. The mass was measured using a calibrated electronic balance. (ASTM International, 2010)

The accuracy of the dial micrometers used here is stated by the manufacture to be 2  $\mu\text{m}$ . This is a 0.008% accuracy on a 25.4 mm measurement. However, when evaluating the uncertainty of the density determination other factors must be considered, such as the hardness of the material and the force with which the micrometer blade is engaged with the material, specimen temperature variation, technician skill, etc. These and other factors were considered in a propagation of error analysis to arrive at an uncertainty of 0.08% with the measurement of the diameter being the largest contributor to the error.

#### **3.2.4.2. Elastic Modulus from Sonic Velocity**

The mechanical properties of graphite are necessary to determine the structural integrity of graphite components. These properties are vital to determining the structural strength and integrity of the reactor core components. The as-received, irradiated, and oxidized property values are required by the ASME BPV code, which will be used as the graphite design code.

Elastic modulus from sonic velocity testing was carried out in accordance with ASTM C769-09. In this measurement the transmitting piezoelectric transducer sends a 2.25 MHz sound wave through the sample. At the opposite end of the sample, the acoustic wave is received by another piezoelectric transducer and the time of flight through the sample is recorded. The sonic velocity of the specimen is calculated from the ratio of specimen length to the signal time lapse between transducers. An approximate value for Young's Modulus,  $E$ , can then be obtained from the following relationship:

$$E = \rho V^2$$

where:

$\rho$  = the specimen density and

$V$  = the sonic velocity.

(ASTM International, 2009)

Figure 3.11 shows the sonic velocity measurement station. In the foreground are the fixtures for clamping the specimen between the transducer and receiver that were specifically designed and fabricated at INL for this application. They have unique features that improve measurement accuracy, precision, and efficiency. For example, measurement precision is improved because the spring-loaded clamp applies consistent pressure between the transducers and specimen resulting in repeatable couplant thickness. The Specimens are easily and rapidly loaded into the fixture using the cam-operated clamp.

As specified in Paragraphs 8.1 and 8.5.1 of ASTM C 769, a suitable coupling medium should be used and reported with the data. Here, "Shear Gel," manufactured by Sonotech Inc., is used for a shear wave couplant and "Ultragel II," also manufactured by Sonotech Inc., is used for the transverse wave couplant.



Figure 3.11: Sonic velocity measurement station.

The uncertainty in determining elastic moduli from the measurement of sonic velocity comes from several sources. First there is the effect of material and geometry related dispersion of the transmitted wave. ASTM C 769 provides guidance on how to minimize this problem by choosing the correct frequency. This technique also assumes linear elastic behavior and graphite is not completely linearly elastic. And finally, the operator's judgment on the placement of the timing

cursors is somewhat subjective. Clean wave forms to base these judgments on are highly dependent on the quality of the transducer-material coupling. These sources of error are difficult to quantify, and therefore difficult to combine in a propagation of error analysis. However, ASTM C 769 describes in some detail a round robin test series between different labs. Using round robin test data to determine a coefficient of variation (COV) is a good means of estimating the measurement uncertainty. With caution, the COV of 3.8% reported in C 769 is taken here to be representative of the uncertainty of these measurements. When considering a single material and making comparisons between the pre- and post-irradiation values, the precision of these measurements is good enough to consider differences greater than 4% significant. However, one is cautioned to refrain from using the values here as absolute, or better than  $\pm 10\%$  accurate.

#### **3.2.4.3. Elastic Modulus from Fundamental Frequency**

The mechanical properties of graphite are necessary to determine the structural integrity of graphitic components. These properties are vital to determining the viability of the structural strength and integrity of the reactor core. This test method measures the fundamental resonant frequency of test specimens of suitable geometry by exciting them mechanically with a singular elastic strike. Specimen supports, impulse locations, and signal pick-up points are selected to induce and measure specific modes of the transient vibration of the specimen. The transient signals are analyzed, and the fundamental resonant frequency is isolated and measured by the signal analyzer. The measured fundamental resonant frequency, specimen dimensions, and mass are used to calculate the dynamic Young's modulus, shear modulus, and Poisson's ratio per ASTM C747-93 (Reapproved 2010) in combination with apparatus and calculations described in ASTM C1259-08. The fundamental frequency measurement station is shown in Figure 3.12.



Figure 3.12: Fundamental frequency measurement station.

After placing a specimen in the test fixture, the user excites it by lightly tapping it with a small mechanical impulse. A consistent impulse is achieved by placing the ball hammer onto a lever that rotates out from under the hammer as it is raised. The specimen is supported in such a way that it vibrates at its natural frequency. A microphone placed underneath one end of the specimen in combination with the Grindosonic electronics measure this frequency, which is recorded and displayed by the computer. The modulus of elasticity is calculated and displayed next to the newly acquired frequency. If the results are satisfactory, the user can press the “Save 1st Frequency” button and go on to the next measurement. Following the recommendations of ASTM C-1259-08, 10 readings of the fundamental frequency are measured before the results of the test are written to the applicable Excel spreadsheet.

ASTM C-1259 describes in detail a round robin test series using ceramic materials along with an analysis of the propagation of errors in the calculation of moduli from the measurement of resonant frequency, geometry, and mass of the specimen. This error analysis shows the major sources of experimental variation are the measurement of the fundamental frequency and the smallest dimension (diameter) of the specimens due to their higher exponent in the modulus calculations. Both the propagation of error analysis and round robin data indicated an uncertainty of less than 2%. However, the specimens tested here do not meet the geometry requirements of C-1259. With a length-to-diameter ratio of only 2, these specimens are, at times, difficult to excite consistently and in a single mode of vibration. Once a resonant frequency is determined by an experienced operator for the flexural mode of vibration, it was easily repeated with accuracy within 2% uncertainty.

#### 3.2.4.4. Coefficient of Thermal Expansion

Measuring the coefficient of thermal expansion (CTE) for graphite components is critical for determining the dimensional changes that occur as a result of temperature cycles. Localized external stresses can be imposed upon mechanically interlocked graphite core components as the individual pieces suffer differential thermal expansion. Internal stresses can occur within larger graphite components if there is a temperature gradient causing differential expansion within the piece (one side has a higher temperature than the other). Finally, the thermal expansion is highly dependent upon the graphite microstructure, such as orientation/anisotropy, pore size and distribution, and crystallinity. Irradiation damage can significantly alter graphite microstructure and thus CTE values. Determining the extent of the changes as a function of irradiation dose and temperature will be a key parameter for reliable calculation of stress states within graphite components, volumetric changes, and irradiation creep rates.

The CTE testing followed ASTM E228-06. This test method uses a push-rod type dilatometer to determine the change in length of a graphite specimen relative to that of the holder as a function of temperature. The temperature is varied over the desired range at a slow, constant heating or cooling rate. The linear thermal expansion and mean coefficient of thermal expansion,  $\alpha$ , are calculated from the recorded data using the following relationship:

$$\alpha = \frac{1}{L_0} \frac{\Delta L}{\Delta T}$$

where:

$L_0$  = specimen initial length

$\Delta L$  = change in length

$\Delta T$  = temperature difference between a specified reference temperature and the temperature at which the change in length was measured.

(ASTM International, 2006)

The Netzsch DIL 402 C commercial system (*Figure 3.13*) currently used at INL does not have the capability to cool the specimen below ambient temperature. Therefore, the initial length at 20°C is

linearly extrapolated from expansion data between 100°C and 150°C and the mean CTE is calculated from a 20°C reference temperature.

The greatest source of experimental error in the dilatometry method described here is the correction made for the expansion of the specimen holder and push rod/LVDT mechanism. This differential between the specimen and the apparatus must be accounted for to isolate the specimen expansion only. Studies reported in the precision and bias section of ASTM E228 have indicated that this type of dilatometry can be accurate to 4% when calibrations are performed carefully.



Figure 3.13: Commercial push rod Dilatometer for CTE measurement.

#### 3.2.4.5. Electrical Resistivity

Electrical resistivity is used as a rapid, simple means to determine the grain orientation, structure, and crystallinity of graphite. In conjunction with optical microscopy, it can be used to determine the microstructural texture of graphite components without much sample preparation work. Resistivity was measured following ASTM C611-98. The measurement technique is commonly referred to as 4-point probe. It consists of passing a known current through the sample and measuring the voltage across the sample at known locations. Based on Ohms law, resistance is determined, and resistivity is calculated from the following relationship:

$$\rho = R \cdot A / L$$

where:

R = the measured resistance

A = the cross-sectional area

L = the length over which the voltage is measured.

The electrical resistivity testing departed from the ASTM standard in a few ways. The size of the oxidized samples constrains the length-to-diameter ratio for resistivity specimens to 2:1. This is smaller than the ASTM recommended ratio of 6:1. Similarly, the gauge length-to-diameter ratio used was 1:1. This is smaller than ASTM recommended ratio of 4:1. Additionally, the standard requires the heating effect on specimen resistivity to be less than 0.1%. However, Section 9 of the standard, Precision and Bias, also describes a maximum precision for this measurement of 0.75%. Therefore, it is not reasonable to require a measurement of the heating effect of less than 0.75%. None of these departures are expected to significantly affect measurements. (ASTM International, 1998)

Figure 3.14 shows a test fixture fabricated at INL that allows a specimen to be rotated for multiple measurements of voltage around its periphery.

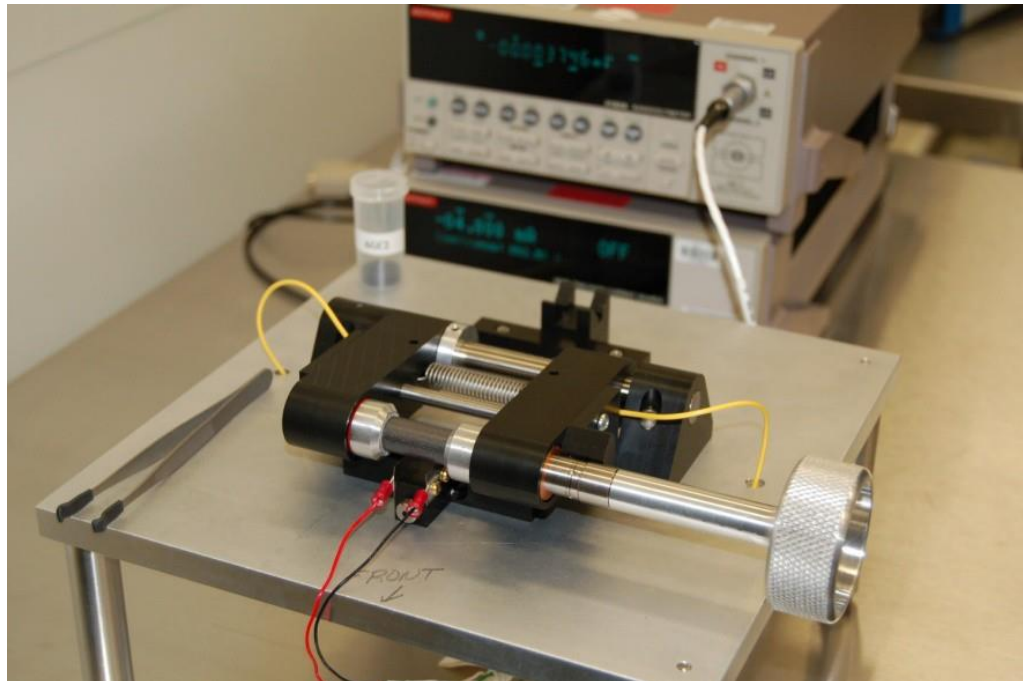


Figure 3.14: Electrical resistivity measurement station.

### 3.2.4.6. Thermal Diffusivity

The ability to conduct heat through the graphite core is critical to the passive removal of decay heat. Reduction of the thermal conductivity within graphite can have a significant effect on the passive heat removal rate and thus the peak temperature that the core and, subsequently the fuel particles, will experience during off-normal events. Determining changes to the conductivity as a function of irradiation dose and temperature is important for the HTGR safety analysis. Here, ASTM E1461-07 was followed for the calculation of thermal diffusivity and conductivity. Thermal diffusivity ( $\delta$ ) is measured and defined as the ratio of thermal conductivity to volumetric heat capacity by the following relationship:

$$\delta = \frac{k}{\rho C_p}$$

where:

k = thermal conductivity

$\rho$  = density

CP = specific heat.

The measurement is performed on small, thin, disk-shaped specimens. A pulsed laser is used to subject one surface of the specimen to a high-intensity, short-duration energy pulse. The energy of this pulse is absorbed on the front surface of the specimen and the resulting rise in rear-face temperature is recorded. The thermal diffusivity is calculated from the specimen thickness and the time required for the rear face temperature to reach 50% of its maximum value. A commercially available LFA, complete with vendor-developed software for instrument control and data acquisition, is used as shown in Figure 10.

Uncertainty in the measurement of thermal diffusivity comes about from specimen heat loss and temperature measurement. Specimen temperature measurement is performed with a calibrated type-S thermocouple in the near vicinity of the specimen. Being relatively straight forward, the specimen temperature measurement is typically a small contribution to the overall measurement error or uncertainty.

The main contributor to the measurement uncertainty is heat loss from the specimen. Because this measurement technique depends on the assumption of one-dimensional heat transfer from

the flat face receiving the laser pulse to the flat face radiating to the detector, heat loss errors are mainly attributed to radiative heat loss from the circumference of the specimen at temperatures above 300°C. Typically provided with the instrument software are several correction models to account for this heat loss. As the specimen diameter to thickness ratio decreases, the heat loss increases to the point that the correction models no longer can account for the error. A study was performed to gain a fuller understanding of the limits of the models made available with the NETZSCH LFA and the dependence of the diameter to thickness ratio on measurement error. In this study, the heat loss models were applied to data taken on specimens with various diameter-to-thickness ratios and at specimen temperatures between 25°C and 1000°C. It was determined that diameter to thickness ratios greater than or equal to 2 resulted in determination of the diffusivity within ASTM E1461 and the manufactures specified uncertainties of 4% and 3%, respectively. (ASTM International, 2007; Swank and Windes, 2014)

The INL LFA measurement station can be seen below in Figure 3.15



Figure 3.15: LFA measurement station for determination of thermal diffusivity.

### 3.3. Results

Results from all mass loss intervals are plotted below. Most plots were normalized to the unoxidized value to more easily compare trends between grades. Coefficient of thermal expansion was not normalized to prevent data point overlap and allow for easier interpretation.

#### 3.3.1. Elastic Modulus from Sonic Velocity

Figure 3.16 shows the shear modulus through sonic velocity for both graphite grades at increasing mass loss values normalized to the respective unoxidized modulus. Figure 3.17 displays the same information for the Young's modulus. These moduli are seen to decrease with increasing oxidation, with IG-110 seeing a slightly more dramatic decrease than NBG-18.

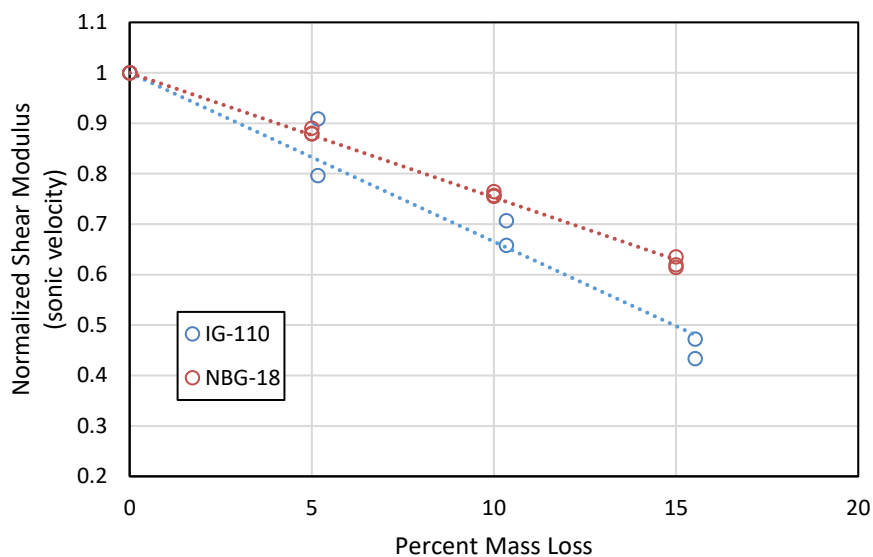


Figure 3.16: Shear modulus from sonic velocity

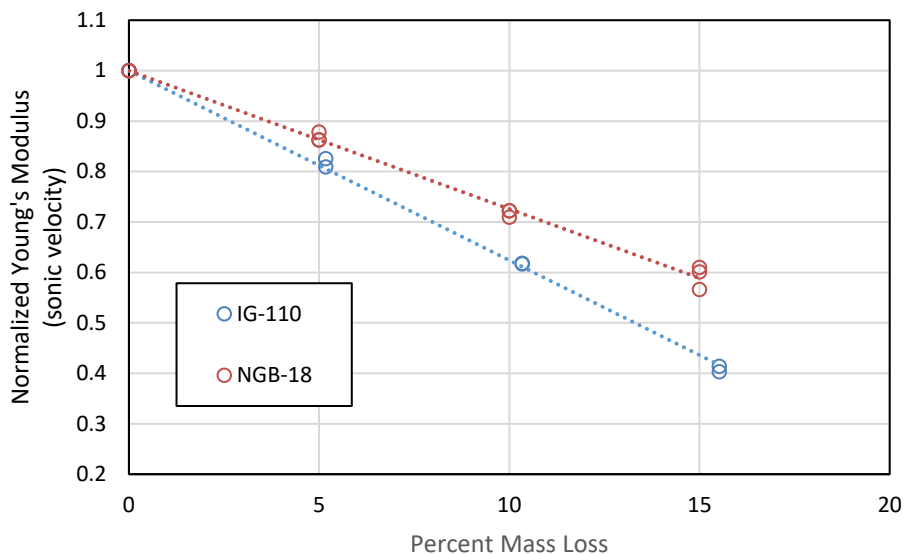


Figure 3.17: Young's modulus from sonic velocity

### 3.3.2. Elastic Modulus from Fundamental Frequency

Figure 3.18 presents the change in Young's modulus from fundamental frequency of the two graphite grades with increasing oxidation normalized to their respective unoxidized modulus value. The decrease in modulus is very consistent with the sonic velocity modulus measurements, with IG-110 seeing a slightly larger decrease than NGB-18.

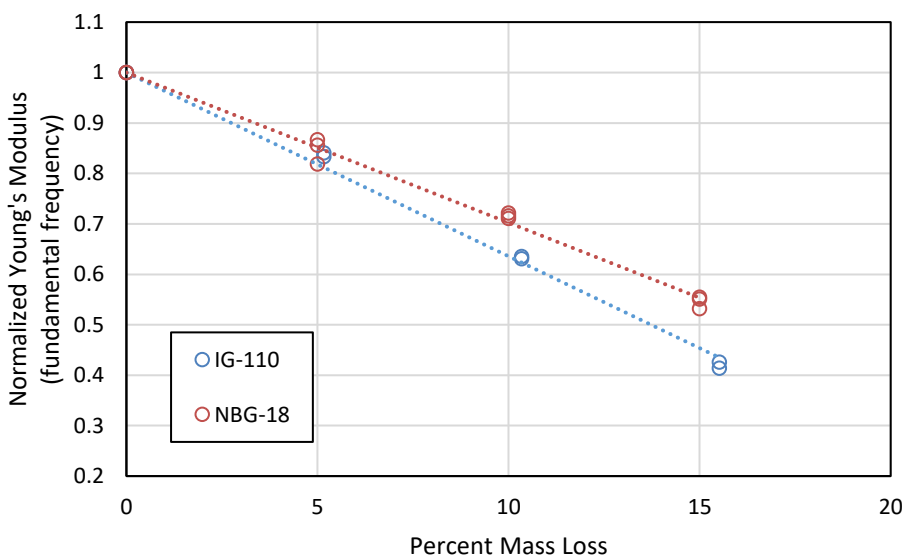


Figure 3.18: Young's modulus from fundamental frequency

### 3.3.3. Coefficient of Thermal Expansion

Figure 3.19 shows the coefficient of thermal expansion of the two graphite grades as a function of temperature for 4 different mass loss values. It is seen that oxidation decreases the coefficient of thermal expansion across all temperatures for both grades. IG-110 sees a much more significant reduction in coefficient of thermal expansion than NBG-18.

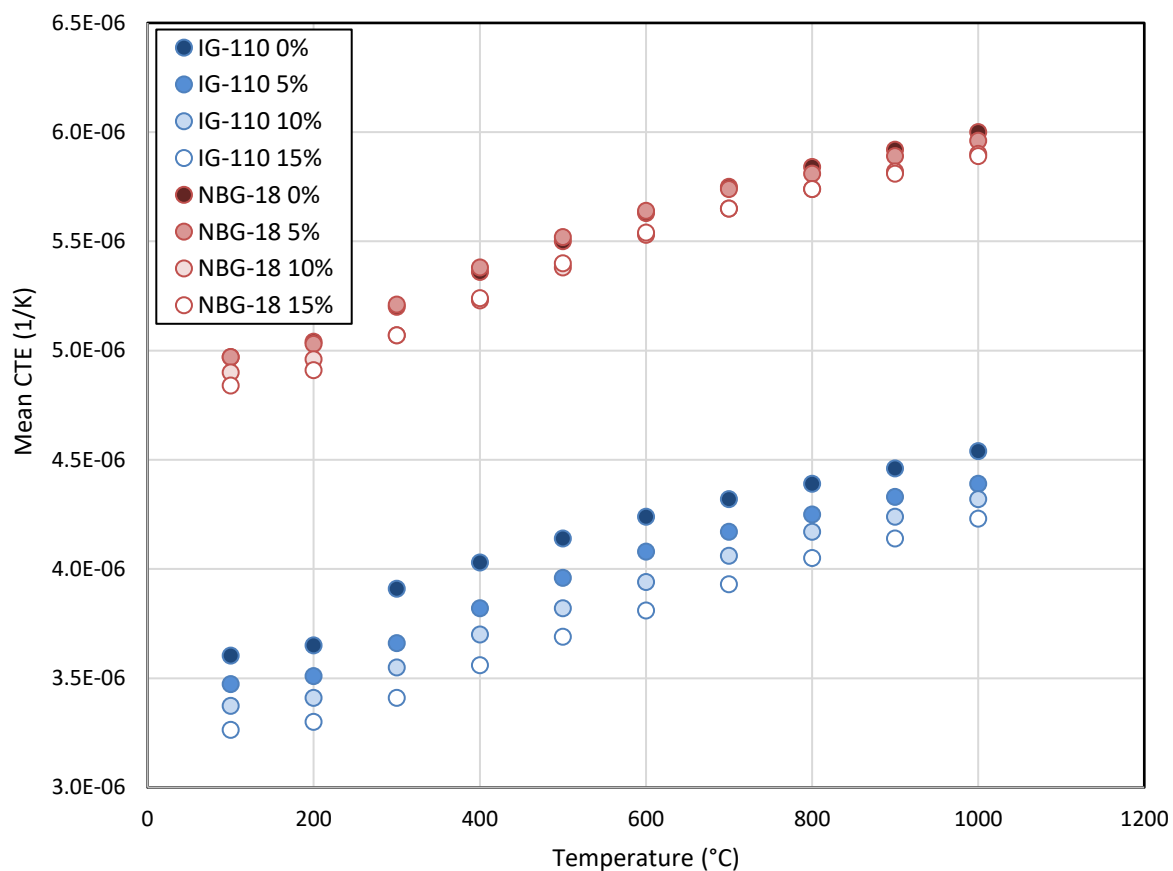


Figure 3.19: Coefficient of thermal expansion

### 3.3.4. Electrical Resistivity

Figure 3.20 presents the change in electrical resistivity of the two graphite grades with increasing oxidation normalized to their respective unoxidized resistivity value. IG-110 experiences a much larger change in relative resistivity than NBG-18.

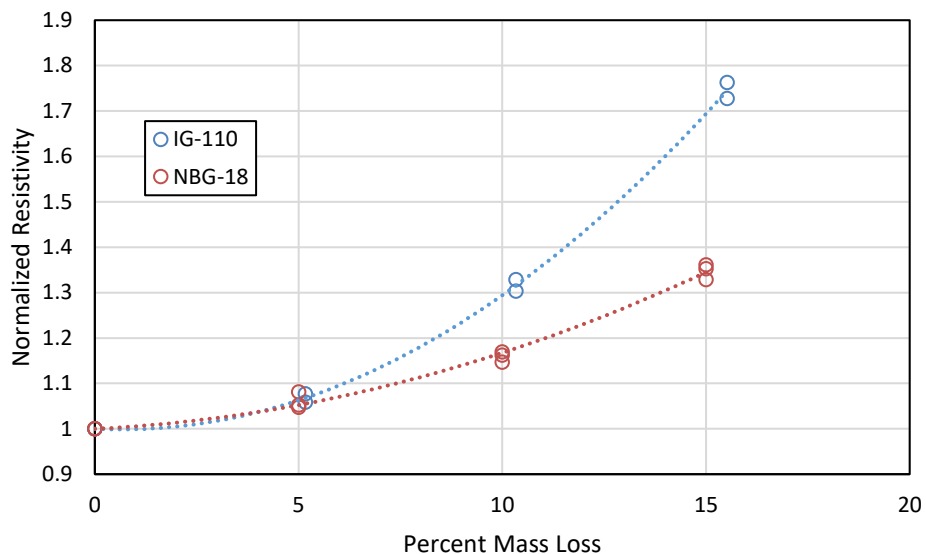


Figure 3.20: Electrical resistivity

### 3.3.5. Thermal Diffusivity

Figure 3.21 shows the normalized thermal diffusivity values of both graphite grades as a function of temperature for multiple oxidation conditions. It is seen that oxidation decreases the thermal diffusivity in all cases, especially at room temperature. IG-110 sees a slightly larger decrease at higher temperatures and higher mass loss values, while NBG-18 sees a larger decrease at room temperature.

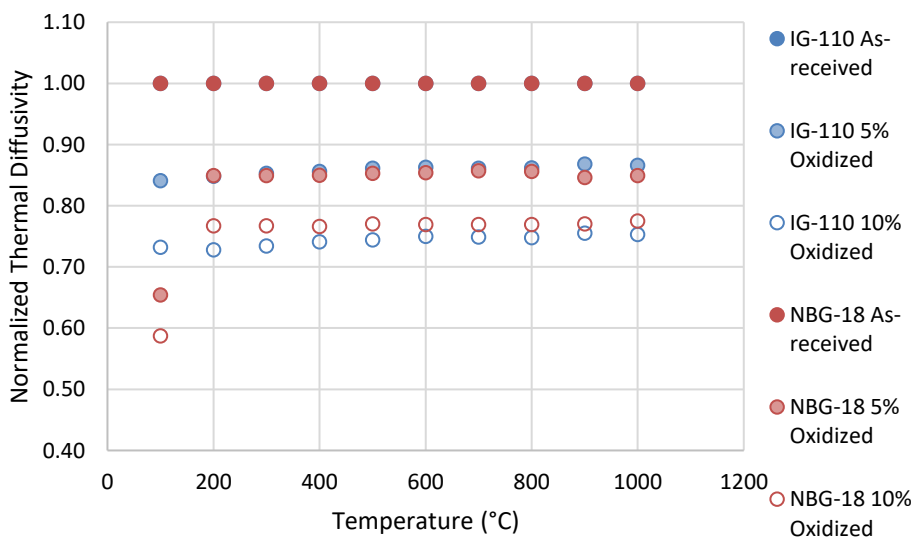


Figure 3.21: Thermal diffusivity through LFA

### **3.4. Discussion**

The graphite material property data are herein discussed. These results are analyzed and compared to previous similar work where applicable.

#### **3.4.1. Elastic Modulus**

Young's modulus and shear modulus trends are consistent between testing methods. Figure 3.16, Figure 3.17, and Figure 3.18 show both moduli decrease linearly with oxidation, with IG-110 seeing a larger decrease than NBG-18. A decrease in modulus means a graphite component will see more deflection under the same load, potentially causing misalignment or shifting in a reactor core. Elastic modulus is also critical to the irradiation response of graphite components. High modulus graphite may generate larger internal stresses from irradiation induced dimensional strain which can lead to crack formation and enhanced crack propagation.

#### **3.4.2. Coefficient of Thermal Expansion**

It can be seen in Figure 3.19 the CTE decreases through all measured temperatures. This is contradictory to prior work on the subject which found the CTE is not affected by oxidation in graphite. (Hacker et al. 2000) The previous oxidation work was done with CO<sub>2</sub> at a much higher temperature (900° C) which has previously been found to cause nonuniform oxidation for samples larger than 0.6 mm where "pore diffusion is incomplete." (Turkdogan et al., 1968) This means the graphite was most likely oxidized in the diffusion-controlled regime, which implies the outer layer of graphite will be highly oxidized while the center of the sample may be entirely unaffected. (Kane et al., 2017) This suggests the CTE testing performed on the samples oxidized at higher temperatures were essentially an intact graphite core wrapped in a layer of higher porosity microstructure and measuring the CTE only captured the values of the intact core. These previous data are illustrated in Figure 3.22.

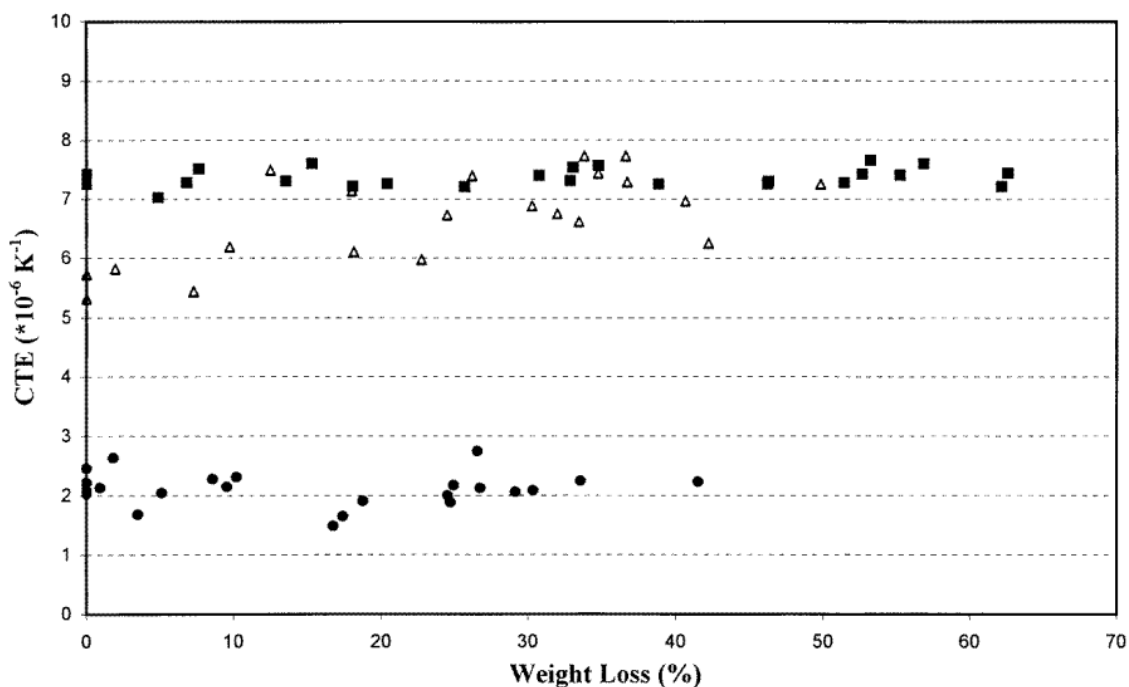


Figure 3.22: Average CTE from 20-600° C as a function of weight loss for 2 different graphites (Hacker et al. 2000)

It should be noted that core components should be sized according to how they will perform in the future, not just at the time of construction. Changes in CTE due to oxidation should be accounted for. A decrease in CTE in nonuniformly oxidized core components may cause significant internal stresses if there are both a significant intact portion and a significant oxidized portion. This needs to be considered by reactor designers and has not previously been identified in literature as a concern.

### 3.4.3. Electrical Resistivity

Figure 3.20 shows the electrical resistivity of graphite with oxidation. A small increase in resistivity is expected as there is less material present to conduct electricity through, however further investigation is needed to determine the cause of the drastic decrease in resistivity observed.

### 3.4.4. Thermal Diffusivity

Normalized thermal diffusivity is seen in Figure 3.21. The decrease in diffusivity with oxidation is consistent over higher temperature ranges where oxidation is more likely to occur. (Kane et al., 2017) The decrease in thermal diffusivity shows higher levels of oxidation in graphite acts more like a thermal insulator than intact graphite. These changes across multiple core components may

result in a decrease in cooling effectiveness which could change local core temperatures. These temperature changes will affect fuel reactivity and need to be accounted for when the neutronic analysis is being performed.

LFA is a well-documented and effective technique for determining thermal diffusivity values and the diffusivity is calculated as

$$\alpha = 0.1388 \frac{L^2}{t_{1/2}}$$

where:

$\alpha$  = diffusivity

L = sample thickness

$t_{1/2}$  = 50% rise time.

(ASTM International, 2007)

This means a small error in sample thickness, L, will result in a large error in diffusivity. As the graphite samples reach higher mass loss values their surfaces become irregular and not perfectly planar. Thickness measurements were taken as accurately as possible, but this is one source of possibly significant error in the diffusivity measurements at higher mass loss values. Analyzing and quantifying this error is beyond the scope of this paper but will be investigated in future work.

### 3.5. Conclusions

This work covered several important physical properties of graphite through a range of different oxidation levels. Additionally, several important results can be observed:

- Changes in thermal diffusivity in oxidized graphite causes graphite to act more like a thermal insulator and change the heat transfer properties of the core, possibly affecting cooling as well as reactivity.
- Nonuniform changes in CTE can result in internal stresses or misalignment in core components that needs to be accounted for in the design of the reactor.
- LFA may not be adequate for measuring thermal diffusivity of graphite at higher mass loss levels due to surface irregularities affecting thickness measurements. Further

research should be conducted into the effects of thickness and the viability of using LFA in these scenarios.

- Uniform oxidation is important for measuring property values as it removes any size or shape dependencies. Uniformly oxidized property values from a range of oxidation mass loss values can then be applied to nonuniformly oxidized components if the gradient of oxidation is known.

### 3.6. References

ASTM International, "ASTM D7542-15 Standard Test Method for Air Oxidation of Carbon and Graphite in the Kinetic Regime," 2015.

ASTM International, "C559-90(2010) Standard Test Method for Bulk Density by Physical Measurements of Manufactured Carbon and Graphite Articles," 2010.

ASTM International, "C611-98 Standard Test Method for Electrical Resistivity of Manufactured Carbon and Graphite Articles at Room Temperature," 1998.

ASTM International, "C747-16 Standard Test Method for Moduli of Elasticity and Fundamental Frequencies of Carbon and Graphite Materials by Sonic Resonance," 2016.

ASTM International, "C769-09 Standard Test Method for Sonic Velocity in Manufactured Carbon and Graphite Materials for Use in Obtaining Young's Modulus," 2009.

ASTM International, "E1461-07 Standard Test Method for Thermal Diffusivity by the Flash Method," 2007.

ASTM International, "E228-06 Standard Test Method for Linear Thermal Expansion of Solid Materials with a Push-Rod Dilatometer," 2006.

Burchell, T., Bratton, R., and Windes, W., "NGNP Graphite Selection and Acquisition Strategy," Oak Ridge National Laboratory, 2007.

Geschwindt, J., Lommers, L., Southworth, F., and Shahrokhi, F., "Performance and optimization of an HTR cogeneration system," *Nuclear Engineering and Design*, vol. 251, 2012.

Hacker, P.J., Neighbour, G.B., and McEnaney, B., "The coefficient of thermal expansion of nuclear graphite with increasing thermal oxidation," *J. Phys. D: Appl. Phys.* 33, pp.991-998, 2000.

Harvego, E.A., Reza, S.M.M., Richards, M., and Shenoy, A., "An evaluation of reactor cooling and coupled hydrogen production processes using the modular helium reactor," *Nuclear Engineering and Design*, vol. 236, pp. 1481-1489, 2006.

Kand, J., Karthik, C., Uvic, R., Windes, W., and Butt, D., "An oxygen transfer model for high purity graphite oxidation," *Carbon*, vol. 59, pp. 49-64, 2013.

Kane, J., Contescu, C., Smith, R., Strydom, G., and Windes, W., "Understanding the reaction of nuclear graphite with molecular oxygen: kinetics, transport, and structural evolution," *J. Nucl. Mater* 493, pp. 343-367, 2017.

Swank, W. and Windes, W., "Specimen Size Effects in the Determination of Nuclear Grade Graphite Thermal Diffusivity", *ASTM Special Technical Papers, STP-2013-0143*, June 2014.

Swank, W., Strizak, J., Lord, J., Burchell, T., Windes, W., "An Inter-Laboratory Comparison of Graphite Testing Procedures", *Transactions of the American Nuclear Society* 106 [1], 2012.

Turkdogan, E., Koump, V., Vinters, J., and Perzak, T., "Rate of Oxidation of Graphite in Carbon Dioxide," Carbon, vol. 6, pp. 467-484, 1968.

## CHAPTER 4. CONCLUSIONS

### 4.1. Strength After Oxidation

It was shown that the strength of nuclear graphite after oxidation is not purely dependent on oxidation mass loss percentage. Samples oxidized to a nominal 10% mass loss retained anywhere from 45 to 85% of their strength depending on grade and oxidation condition. Higher temperature oxidation tends to result in higher retained strength as damage is not able to penetrate the graphite, leaving an intact center region of high strength. Lower temperature oxidation tends to result in lower retained strength, as the damage is distributed throughout the graphite and critical flaws are increased in size. These trends were seen both in the results from mechanical testing of the samples as well as the optical analyses of oxidized samples across the temperature range. Sample trimming was found to be a necessary part of mechanical testing of oxidized graphite, both to leave flat and planar ends for the contact blocks in the load frame and to remove a region of higher damage from the ends of the samples. Testing of untrimmed samples tends to result in premature failure on the edges of the untrimmed surfaces and inconsistent results. Trimming resulted in more consistent results and was verified using optical analysis.

### 4.2. Properties After Oxidation

Several important points were made regarding the thermal and physical properties of oxidation. Uniform oxidation is essential for conducting property measurements to remove any size or shape effects. Testing non-uniformly oxidized specimens will give results that are dependent on the gradient of oxidation and will therefore be inconsistent. Property measurements from uniformly oxidized samples over range of oxidation conditions can then be applied to non-uniformly oxidized graphite components in a piecewise manner to estimate the overall properties of the entire component. The coefficient of thermal expansion of graphite changes when it is oxidized, meaning non-uniform oxidation of a graphite component that sees elevated temperatures may experience unexpected internal stresses. This does not agree with previous work that performed measurements on non-uniformly oxidized samples and found no change in coefficient of thermal expansion with increasing oxidation. The thermal diffusivity of graphite decreases with increasing oxidation, meaning graphite may begin to behave as more of a thermal insulator than a conductor. This can lead to increased localized temperatures in reactor which will affect reactivity.

Additionally, it was found that laser flash analysis may not be the best method for measuring thermal diffusivity of graphite after oxidation due to its high sensitivity to thickness variabilities in samples. The rough surface of oxidized graphite may change the path length for the energy to travel through the sample, resulting in measurement errors. Other techniques should be utilized in parallel with laser flash to determine its accuracy for degraded graphite surfaces, but such a study is beyond the scope of this work.

#### **4.3. ASME BPV Code Concerns**

The overlying concern discovered with the ASTM BPV code is that the conditions for oxidation are not specified. It was shown that the strength of graphite is not simply a function of mass loss but also of oxidizing condition. Graphite may oxidize uniformly resulting in damage throughout the structure and severely decreased strength, or it may oxidize non-uniformly which may not have an effect on the thermal and physical properties and has much less of an effect on the retained strength. This is highlighted by the conflicting results between the measurements performed here on uniformly oxidized samples and previous work on non-uniformly oxidized samples.

The current assessment in the ASME BPV code excludes all graphite from the stress assessment after it has reached an oxidation mass loss of roughly 10%. This was found to be a fairly accurate assessment for small, uniformly oxidized samples, but it is likely too conservative for samples oxidized at higher temperatures where the damage is not uniform and the graphite can retain over 80% of its strength. This is an easy distinction to make when testing samples that fit in the palm of your hand but gets more complicated when looking at all the graphite components in a reactor. The code currently does not provide guidance on how oxidation mass loss is to be measured. Measuring mass loss on a whole core basis would be problematic, as the areas of higher temperature would oxidize more quickly assuming a uniform distribution of oxidants. Measuring on an individual component basis would be more accurate but again, some components are quite large and there would be localized oxidation at regions of higher temperatures. Another option would be to look at the graphite in discrete volumes, but the sizing of volumes and measurement of oxidation may be prohibitively difficult. The task of quantifying how the real-world strength of reactor components is affected by oxidation is difficult but there needs to be a standard method backed by real data.